Strengthening of reinforced concrete beams with insufficient lapped splice length of reinforcing bars

Engineering Structures 321 (2024) 118922

Contents lists available at ScienceDirect

Engineering Structures

journal homepage: www.elsevier.com/locate/engstruct

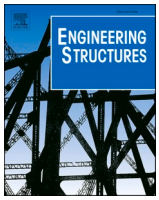

Strengthening of reinforced concrete beams with insufficient lapped splice length of reinforcing bars

Mohamed Ghalla [a], Moataz Badawi [b], Galal Elsamak [a,c], Mizan Ahmed [d], Qing Quan Liang [e,*,1], Mohamed A. El Zareef [b,f]

[a] Civil Engineering Department, Faculty of Engineering, Kafrelsheikh University, Kafrelsheikh, Egypt
[b] Civil Engineering Department, College of Engineering and Architecture, Umm Al-Qura University, Makkah, Saudi Arabia
[c] Civil Engineering Department, Delta Higher Institute for Engineering and Technology, Mansoura, Egypt
[d] Centre for Infrastructure Monitoring and Protection, School of Civil and Mechanical Engineering, Curtin University, Kent Street, Bentley, WA 6102, Australia
[e] College of Sport, Health, and Engineering, Victoria University, PO Box 14428, Melbourne, VIC 8001, Australia
[f] Structural Engineering Department, Faculty of Engineering, Mansoura University, Mansoura, Dakahlia 35516, Egypt

ARTICLE INFO

Keywords:
Externally bonded reinforcement
Finite element modeling
Lapped splice
Near surface mounted
Prestressing
Reinforced concrete
Stainless-steel sheets
Strengthening

ABSTRACT

The insufficient lapped splice length of reinforcing bars due to the design or construction errors reduces both the flexural strength and ductility of Reinforced Concrete (RC) beams. The defected RC beams need to be strengthened to allow structures to be ductile and robust in their design life. This paper reports experimental and numerical investigations into the flexural behavior of RC beams having insufficient lapped splice length of reinforcing bars strengthened by various techniques. Eleven RC beams have been tested to examine the effects of strengthening techniques and anchorage lengths of the strengthening materials on the performance of the beams. The test program and results are described on RC beam specimens strengthened by using the externally bonded stainless-steel (EBSS) sheets, the near surface mounted (NSM) steel bars, and the external prestressing system. Finite Element (FE) models are developed using ABAQUS to simulate the responses of strengthened RC beams in which the lapped splice length of reinforcement is inadequate. A parametric study is conducted using the validated FE models to examine the effects of the length of EBSS sheets and steel anchor bolts at the ends on structural behavior. An analytical model is proposed for calculating the ultimate capacity of beams strengthened by NSM technique. Experimental results reveal that the proposed strengthening methods can significantly improve both the cracking and ultimate loads of the defected beams. The application of the external prestressing method results in the largest increase in the cracking and ultimate loads of the defected beams calculated as 222 % and 213 %, respectively compared to the defected control beam. The ultimate load of the defected beam strengthened with EBSS sheet, NSM steel bars, and prestressing system with a length of 100D increases by 50 %, 109 %, and 182 %, respectively. It is shown that the developed FE models can accurately predict the behavior of strengthened beams having inadequate lapped splice length of reinforcing bars. The parametric study demonstrates that strengthening the entire clear span of the beam B-ESS-65D with EBSS sheet increases its ultimate load by 207 %. The failure mode of strengthened beams is ductile bending without debonding. The proposed analytical model is shown to yield accurate calculations of the ultimate loads of strengthened RC beams.

1. Introduction

The lapped splices of reinforcing bars are frequently used in reinforced concrete (RC) members that are longer than the supplied length of reinforcing bars [1–3]. To effectively transfer the stress in a structural lapped splice, the length of the lapped splice of reinforcing bars must be adequate. Empirical equations for determining the required lapped splice lengths were developed based on test data [4,5]. AS3600–2018 [6] requires that the lapped splice length of reinforcing bars must be greater than 1.25 times the development length of the bar. ACI 318–19 [7] also specifies the minimum lengths of lapped splices as well as provides a formula for calculating the lapped splice length based on the

* Corresponding author.
E-mail address: Qing.Liang@vu.edu.au (Q.Q. Liang).
[1] https://orcid.org/0000-0003-0333-2265.

https://doi.org/10.1016/j.engstruct.2024.118922
Received 19 November 2023; Received in revised form 9 June 2024; Accepted 2 September 2024
Available online 14 September 2024

required anchorage length of the bar. However, reinforced concrete beams might be constructed with insufficient lapped splice length of reinforcing bars due to either the design error or the construction error. The insufficient lapped splice length leads to a reduction in the strength and ductility of reinforced concrete beams. These defected beams need to be strengthened to restore their strength and ductility. Therefore, there is an urgent need to undertake experimental and numerical studies on the behavior of strengthened RC beams having inadequate lapped splice length of reinforcement.

Some studies have been performed previously to evaluate the effectiveness of various strengthening methods for reinforced concrete beams with insufficient lapped splices [4,8–10]. Juntanalikit et al. [11] studied experimentally and numerically the strengthening of non-ductile RC columns with and without lapped splice. The observation revealed that a lapped splice having inadequate length leads to a reduction in the strength of RC columns and a sharp decline in the post-peak curve. Additionally, the lapped splice contributes to the expansion of the damaged zone. The bond performance of substandard lapped splices in RC beams externally confined with CFRP was examined by Garcia et al. [12]. They reported that the confinement provided by CFRP improved the bond strength of lapped splice by up to 65 % compared to unconfined beams.

A variety of techniques have been employed previously to strengthen concrete elements with defects. One of the commonly used techniques is the Externally Bonded Reinforcement (EBR), including bonding steel plates [13–15], fiber-reinforced polymer sheets, or other materials [16, 17]. The strengthening materials provide additional flexural and shear strength to the beam [18]. The application of Stainless-Steel Sheets (SSSs) is considered one of the best sustainable strengthening techniques that significantly improve the performance of structural elements [19–22]. Design rules for the use of SSSs in construction can be found in international building codes [23–25]. Franco et al. [26] studied the behavior of concrete T-beams which were strengthened by using SSSs. The study explored the effectiveness of bonding techniques using EBR and Near Surface Mounted (NSM) in strengthening RC T-beams. The results revealed that the NSM strategy demonstrated superior performance, achieving a maximum bond stress that was 147.7 % higher than the EBR one. The SSSs were used to strengthen RC curved beams by researchers [27,28]. It was shown that the SSSs enhanced the elastic index and absorbed energy by about 50–150 % compared to the control specimen.

The NSM strengthening technique has gained significant attention in recent years as an effective method to enhance the structural performance of existing concrete elements. One of the key advantages of the NSM technique is its ability to provide improved bond behavior between the strengthening material and the surrounding concrete [29,30]. The NSM approach promotes a more efficient load transfer mechanism, thereby enhancing the resistance against various types of loading, such as flexure [31] and shear [32]. Experiments and numerical studies demonstrated that the NSM strengthening technique increased the load-carrying capacity, stiffness, and ductility of RC beams [33–35]. It was found that the NSM technique effectively mitigated premature failure modes of RC beams, such as debonding and splitting, which were commonly observed in beams repaired by the EBR techniques [36]. Furthermore, the NSM technique offers advantages in terms of aesthetics and durability [37]. Al-Issawi and Kamonna [38] studied the performance of RC deep beams strengthened by NSM steel bars. The test findings demonstrated a substantial increase in the ultimate strength of the tested beams by 7.35 % to 20.6 %.

The use of prestressing systems to strengthen RC beams has gained significant attention in structural engineering [39]. This technique not only significantly enhances the load-carrying capacity and ductility of RC beams but also reduces their deflections and cracking [40,41]. In addition, the prestressing technique can counteract tensile stresses and provide a more balanced stress distribution [42]. Miao et al. [43] utilized prestressed NSM steel wire ropes to improve the flexural performance of stone slabs. The technique was found to improve the flexural strength of the strengthened specimen. The improvement of the flexural strength of the slabs increased with an increase in the prestressing force.

A number of researchers studied the strengthening of RC beams having lapped splices with insufficient length of reinforcing bars. Sayed and Elrakib [44] experimentally studied the behavior of RC beams with insufficient lapped splice length of longitudinal reinforcement that were strengthened using transverse and longitudinal FRP sheets. One of the tested specimens was strengthened with longitudinal FRP sheets while five beams were retrofitted with transverse FRP sheets; Four control beams were tested for comparison purposes. The study variables were the compressive strength of concrete, the type of FRP sheets, the length of the strengthened zone as a proportion of the internal lapped splice length, and the configuration of the FRP. The test results showed that the use of transverse FRP sheets increased the confining stress on the concrete, which improved the stress transfer between the reinforcing bars and the concrete and ultimate loads of the beams which experienced ductile collapse pattern.

Beiter [45] tested four RC beams, two of which were control ones. The first beam had sufficient lapped splice length of longitudinal reinforcement to meet the requirement of ACI 318–71 [46]. The lapped splice length of longitudinal rebars in the second beam was half of that in the first beam. Two other beams similar to the second beam were strengthened using different layouts of post-installed anchors. It was observed that strengthening using post-installed anchors increases the ultimate capacity and ductility of defected beams.

Dagenais and Massicotte [47] used ultra-high-performance fiber--reinforced concrete (UHPFRC) to strengthen tension lapped splices in RC beams made of normal strength concrete. They investigated the effects of various parameters on the performance of strengthened RC beams, including the length of the splice, the diameter of the inner reinforcing bar, the depth of the strengthening zone, and the location of the inner reinforcing bars. It was reported that strengthening the splice zone with an appropriate depth of UHPFRC can increase the bond stresses of the reinforcing bars in the splice zone and avoid collapse by splitting.

Abdallah et al. [48] conducted a study on strengthening RC beams where the lapped splice length of reinforcing bars was not adequate. This was achieved by adding a ferrocement Engineered Cementitious Composite (ECC) layer of varying lengths, utilizing different techniques such as a cast-in-situ layer, a cast-in-situ layer reinforced with steel anchors, and a precast layer reinforced with steel anchors. The study revealed that the use of an anchored cast-in-situ ECC ferrocement layer, with an anchorage length of 50D (where D is the diameter of the embedded reinforcing bar in the splice), increased the cracking load by 137 % and the ultimate load by 164 % compared to control beam. The failure pattern also changed from slippage of the bars in the splice to flexural failure.

However, there is still a deficiency in the study of the responses of strengthened RC beams containing insufficient lapped splice length of reinforcing bars. This paper is concerned with the strengthening of RC beams where the lapped splice length of reinforcing bars is not adequate. Debonding is the most common failure mode of RC beams strengthened using the EBR technique. To overcome this problem, previous studies have shown that additional steel anchors or longer strengthening sheets can be used. Therefore, in the current study, the effects of various strengthening techniques on the performance of RC beams with lapped splices are investigated.

The current study presents alternative methods that address the shortcomings of other strengthening techniques in previous studies. One of these methods involves using SSSs externally bonded to the beam surface at the defective lap splice, either with or without steel shear connectors using an epoxy adhesive. This method has several advantages, including: (1) its fire resistance when using steel shear connectors compared to the use of FRP [44], and (2) not increasing the dimensions

of the beam section as a result of the strengthening process compared to casting an additional layer of ferrocement composites [48]. However, a drawback of the strengthening method using SSSs, similar to that of FRP strengthening, is the occurrence of debonding failure of these sheets. Therefore, other alternative methods were presented, such as the strengthening method using NSM, which involves embedding additional steel bars with bent ends (not included in [47]) into a layer of ECC. The previously mentioned strengthening methods, whether using SSSs, NSM, or those mentioned in [44], [47], [48], require a sufficient length of strengthening to transfer bonding stresses between the strengthening material and the beam without debonding. Therefore, the final method presented in the current study uses a technique that does not require a large strengthening length, namely, the use of externally post-tensioned steel bars.

Tests on eleven defected RC beams under three-point loads have been conducted to quantify the effects of anchorage lengths and various strengthening methods on the structural behavior. The paper is structured as follows. The experimental program is described in detail in Section 2 and the results obtained are discussed in Section 3. In Section 4, nonlinear finite element (FE) models are developed by using ABAQUS to simulate the performance of tested beams and verified by test data. Section 5 presents a parametric study of strengthening using EBR technique, using different lengths of SSSs and adding steel anchor bolts at the ends. Section 6 presents an analytical model to calculate the ultimate capacity of RC beams with insufficient lapped splice length of reinforcing bars strengthened with NSM technique. Important concluding remarks are provided in Section 7.

2. Experimental program

2.1. Specimen details

The experimental program was designed to study the flexural behavior of RC beams with insufficient lapped splices strengthened with different techniques. Eleven beams were tested up to collapse with specifications summarized in Table 1. The beam specimens were strengthened by either the externally bonded reinforcement (EBR) stainless-steel sheets, the near surface mounted (NSM) steel bars, or the external prestressing system.

Table 1
Details of the tested specimens.

Group	Beam	Strengthening technique	Anchorage Length (L_a)	Size of SSSs / steel bars diameter
G1	B0	Master beam	————	————
	DB	Defected beam	————	————
G2	DB	EBR SSSs	————	————
	DB-SS-40D		400 mm	50 × 1.0 mm
	DB-SS-50D		500 mm	
	DB-SS-60D		600 mm	
G3	DB	NSM steel bars	————	————
	DB-S-40D		40D (400 mm)	10.0 mm
	DB-S-50D		50D (500 mm)	
	DB-S-60D		60D (600 mm)	
G4	DB	External prestressing system	————	————
	DB-Pr-40D		40D (400 mm)	10.0 mm
	DB-Pr-50D		50D (500 mm)	
	DB-Pr-60D		60D (600 mm)	

All tested beams had identical dimensions with cross-section of 100 × 200 mm and a length of 1500 mm, as shown in Fig. 1. Two deformed steel bars with 10-mm diameter were placed at the top and bottom of the beam as longitudinal reinforcement. The master beam was reinforced with continuous longitudinal bars without lapped splices as shown in Fig. 1(a). When designing beam B0, it was considered that the collapse load in shear should be four times the collapse load in bending. Based on AS3600–2018 [6], the required minimum lapped splice length of 10-mm diameter reinforcing bars with yield stress of 360 MPa in the concrete with $f_c^{'} = 25.35$MPa was calculated as 339 mm. A lap length of 100 mm for the bottom reinforcing bars was used in both the defected beam and the nine strengthened beams as illustrated in Fig. 1(b). Therefore, the lapped splice length of 100 mm was not adequate for the reinforcing bar to develop its yield strength.

As shown in Table 1, the first Group consisted of two beams, one was a master beam (non-defected) and the other was the defected RC beam with insufficient lapped splices. In Table 1, 'DB' refers to defected beam; 'SS' refers to stainless steel sheet; 'S′ refers to steel bar; 'P_r' refers to beams prestressed and '40D/50D/60D' refers to the anchorage lengths (L_a) measured from the mid-span to the end of the strengthening bars/sheet, where D is the bar diameter. The total length of the strengthening bars/sheet were 800 mm, 1000 mm, and 1200 mm. All strengthened beams were named A-B-C where A is the type of beam; B is the strengthening technique; and C is the anchorage length. For example, DB-SS-50D, strengthening of the defected beam with SSSs used herein with L_a of 500 mm. The second Group consisted of three beams with the same geometry to study the impact of the EBR strengthening strategy using SSSs as shown in Fig. 2(a). Three beams, namely DB-SS-40D, DB-SS-50D, and DB-SS-60D, were prepared to have a L_a of 400 mm, 500 mm, and 600 mm, respectively, as depicted in Fig. 2(a) and Table 1. The third Group was designed to investigate the NSM strengthening scenario using additional deformed steel bars. The fourth Group focused on the effect of applying the post-tensioning system as an external strengthening technique. As presented in Fig. 2(c), three tested beams were examined, which were DB-Pr-40D, DB-Pr-50D, and DB-Pr-60D.

2.2. Material properties

Two concrete mixes namely Normal Concrete (NC) and Engineered Cementitious Composite (ECC) were used to cast the test specimens. The mix proportions for each type were the same as the one reported earlier [28]. All tested beams were cast with NC while the ECC was used as filling material to cover the NSM steel bars tested in G3. The ECC mix is characterized by high-strain hardening performance.

Three concrete cylinders with 150 × 300 mm were tested to obtain the compressive strengths ($f_c^{'}$) for each concrete mix on the same day of the beam testing. The compressive strength of NC and ECC concrete was measured as 25.35 and 45.25 MPa, respectively. In order to capture the tensile strength for the two concrete blends, uniaxial tensile tests were undertaken with dog-bone specimens with doubling dimensions given by ACI recommendations [7] as shown in Fig. 3(a). The tensile strength of NC and ECC was measured as 2.61 and 6.25 MPa, respectively. The measured stress-strain relationships for both concrete mixes were idealized as shown in Fig. 4 using the recommendation given by Ge et al. [49].

Fig. 5 presents the uniaxial tensile test that was prepared to measure the material properties of the used steel elements. The actual stress-strain curves are shown in Fig. 6.

2.3. Casting and strengthening preparation

All beams were cast with normal strength concrete using wooden formworks as shown in Fig. 7(a). In the preparation of the beam with SSSs, the bottom surface of the beam was roughened, as depicted in Fig. 8(a). Subsequently, Sikadur 31 epoxy was used to bond the SSSs to

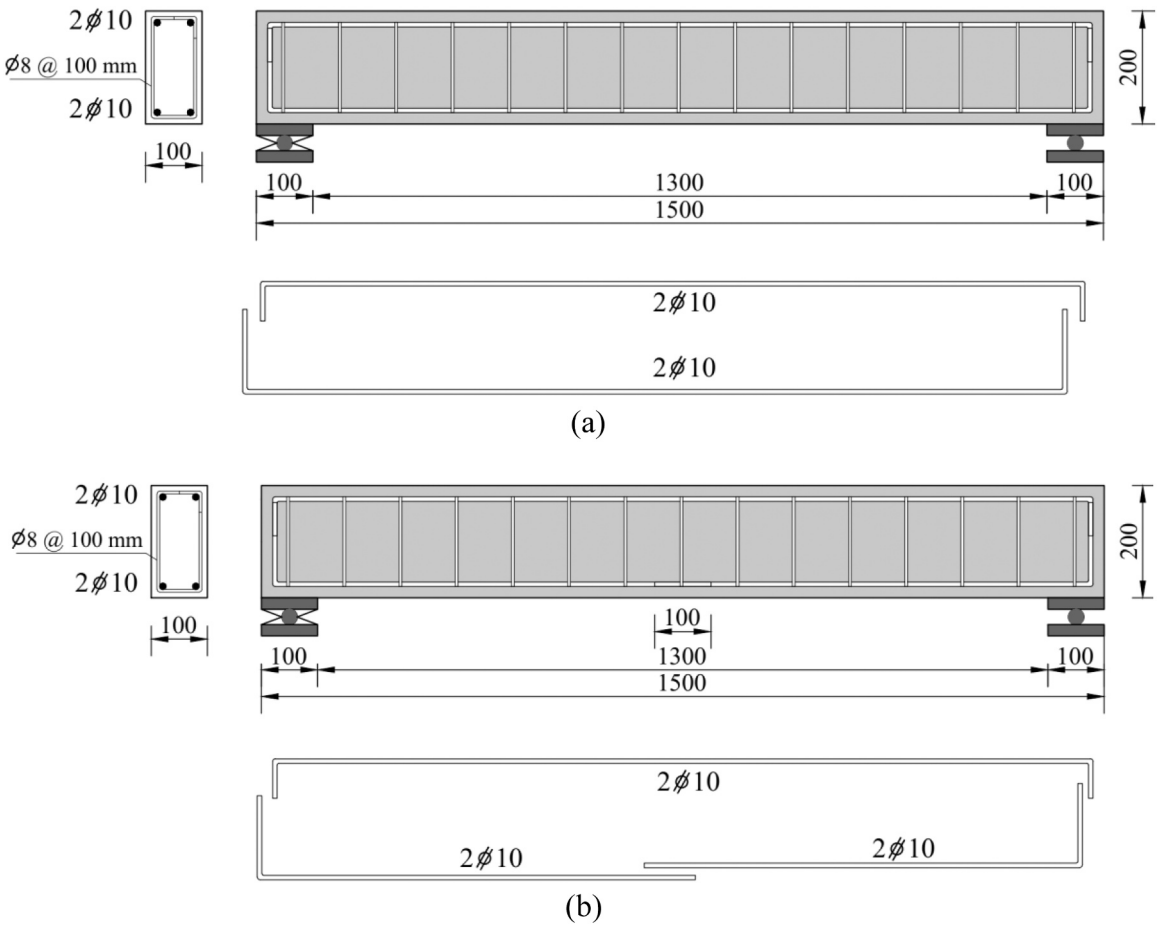

Fig. 1. Geometric and reinforcement details of the beams: (a) Master beam; and (b) Defected beam. (Units: mm).

the concrete externally, as shown in Fig. 8(b). These SSSs were symmetrically placed 50 mm wide in the center of the bottom face of the beam with length L_a varied from 40D to 50D, and 60D. For beams in Group G3, the NSM deformed steel bars were used to strengthen the beams. A wide groove with a width of 50 mm was made in the cover concrete. The additional deformed steel bars were then inserted in the cover concrete using a chemical epoxy adhesive material with a 50 mm embedded length, as depicted in Fig. 9(a). Then ECC was employed to cover, shape, and level the outer concrete cover. For beams strengthened with a simple post-tensioning technique, two fixed-end rigid steel plates with one hole at each end were positioned just upper the main steel bars pathing the two sides of the beam as shown in Fig. 2(c). Screwed steel bars were then positioned as shown in Fig. 2(c). The screwed steel bars were inserted through the holes in the plates respecting to L_a summarized in Table 1 as shown in Fig. 10. At each end of the bars, two nuts were inserted and then tightened to initiate the prestressing force. A strain gauge was used to determine the prestressing force, as depicted in Fig. 10. The value of the prestressing force was 10.50 kN equal to the cracking force of the master beam B0.

2.4. Loading arrangement, test setup, and instrumentation

All beam specimens were tested under three-point loads at the structural laboratory of Kafrelsheikh University, Egypt. The schematic diagram of the test setup is shown in Fig. 11(a). Fig. 11(b) illustrates the configuration of the actual test setup. The load was applied to the top of the beam at the mid-span with displacement control as shown in Fig. 11 (a). A hydraulic jack attached to a steel counterforce frame was employed to apply the load. As shown in Fig. 11, a single Linear Variable Displacement Transducer (LVDT) was attached to the mid-span of the tested beam to measure the vertical deflection. A load cell with a capacity of 1000 kN was equipped with instrumentation to measure load. A digital data logger was employed for the data acquisition. The load was incrementally applied, and the occurrence and spread of cracks were monitored until the specimen collapsed.

3. Test results and discussions

Table 2 summarizes the test results obtained from the experimental program. In Table 2, P_{cr} refers to the first cracking load; Δ_{cr} refers to the deflection at the first cracking load; P_u refers to the ultimate load; Δ_{Pu} refers to the deflection at the ultimate load; K refers to elastic index; E refers to absorbed energy; O refers to overlapping failure; F refers to flexural failure; D refers to debonding.

3.1. Failure modes and crack patterns

During the initial loading phase, the master beam (B0) showed no signs of deformation. The first hair crack was found to emerge at the mid-span of the beam when a load of 10.50 kN (approximately 29 % of the ultimate load capacity, P_u) was applied, as depicted in Fig. 12(a) and summarized in Table 2. Subsequently, additional hairline cracks similar to the first one appeared on the tension side. With the progression of the load, these cracks extended and moved upward toward the top of the beam. Furthermore, they widened and became more pronounced. Just before the beam failed, the inclined shear flexural cracks developed at a loading stage that corresponded to approximately 86 % of its ultimate capacity, as shown in Fig. 12(a). Importantly, these inclined cracks shifted diagonally towards the upper compression side, where the load was applied. Ultimately, the beam could not sustain any further load,

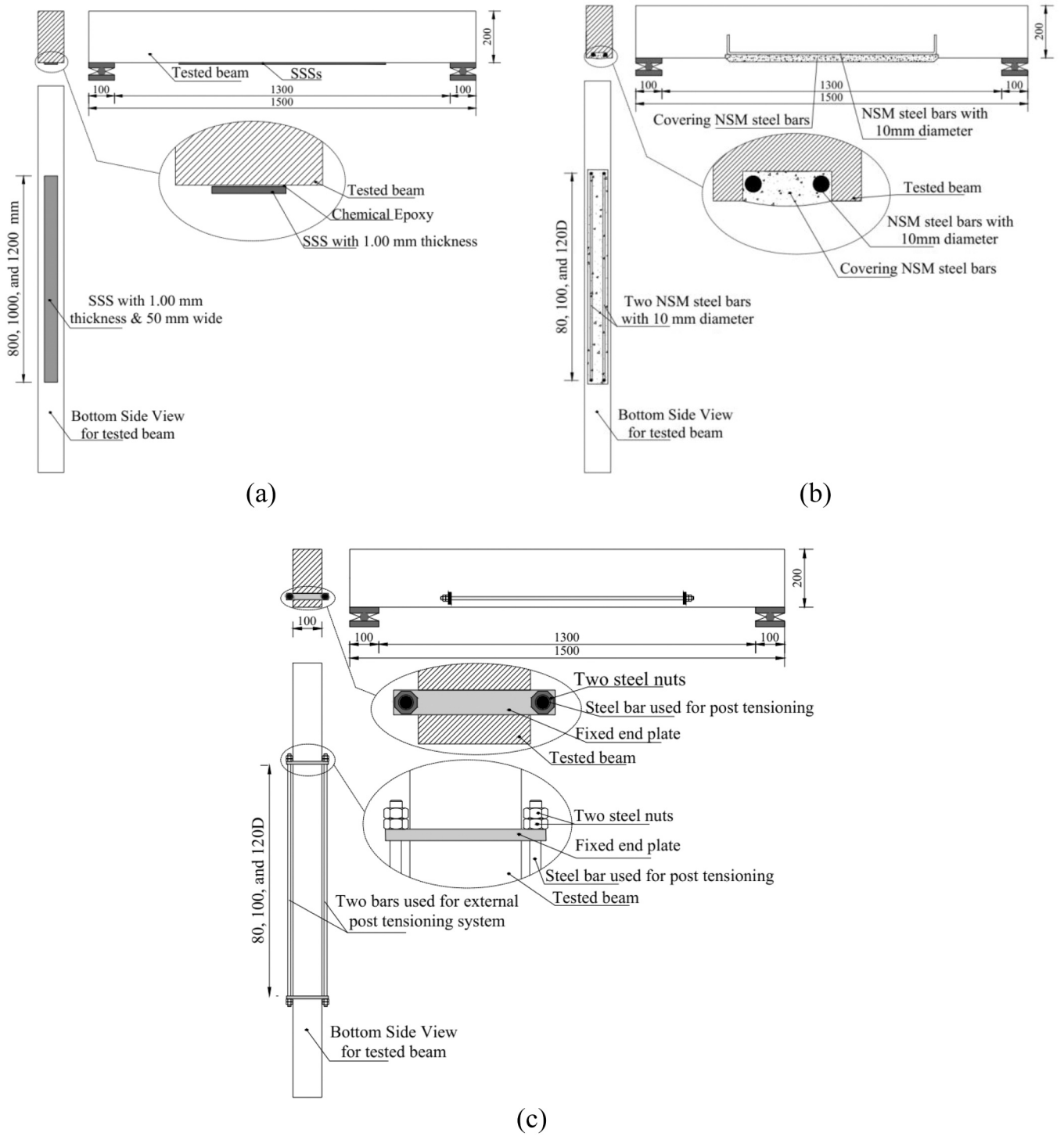

Fig. 2. Geometry of the tested beams: (a) Group G2, (b) Group G3, and (c) Group G4.

resulting in the sudden crushing of the concrete in the loading region. The ultimate load of the beam B0 was recorded as $P_u = 36.55$ kN as provided in Table 2. The failure of the beam was purely due to tensile stresses, and it was followed by crushing of concrete in the compression zone, as depicted in Fig. 12(a). However, only a few crakes appeared on the defected beam (DB) compared with the master counterpart, as shown in Fig. 12(b). The first visible hair crack developed at the mid-span of the beam when a load of 5.04 kN (about 33 % of P_u) was applied, as tabulated in Table 2 and shown in Fig. 12(b). Another parallel vertical crack developed beside the first one from the tension side upward toward the loading region. A horizontal hair crack appeared at the overlapping zone of the main steel bars just before failure. Finally, due to excessive tensile stresses, a sudden failure occurred at the lapping zone. The ultimate capacity (P_u) of the beam was 15.20 kN which is 58 % lower than that of the master one.

The second Group was designed to examine the EBR strengthening strategy using sustainable SSSs. The crack patterns of the three collapsed beams are shown in Fig. 13 for collapsed beams DB-SS-40D, DB-SS-50D, and DB-SS-60D. The initial occurrence of the first hair crack appeared at the mid-span of the specimens when subjected to loads of 7.52 kN,

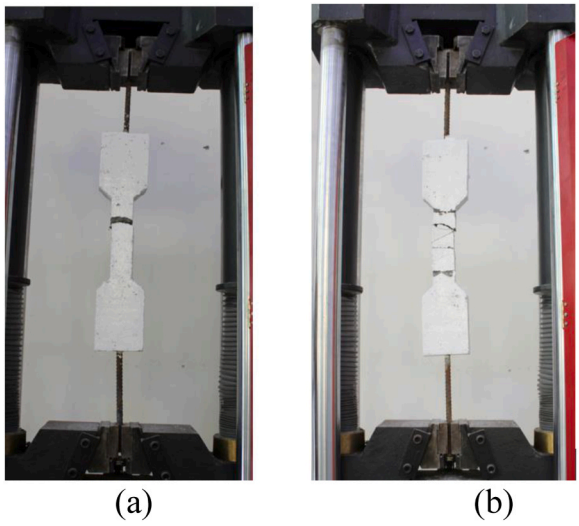

Fig. 3. Uniaxial tensile test for concrete: (a) NC and (b) ECC.

7.86 kN, and 8.01 kN, respectively. The utilization of SSSs resulted in an approximate increase of 49 %, 56 %, and 59 % in the cracking load (P_{cr}) compared to the defected control beam. However, when compared to

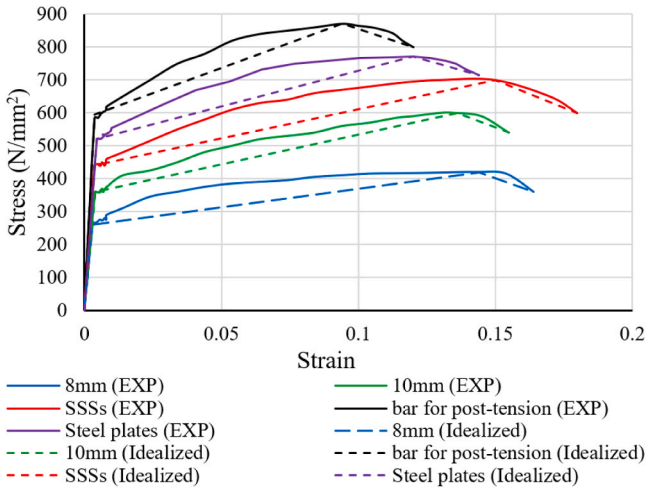

Fig. 6. Measured and idealized stress-strain curves of steel components.

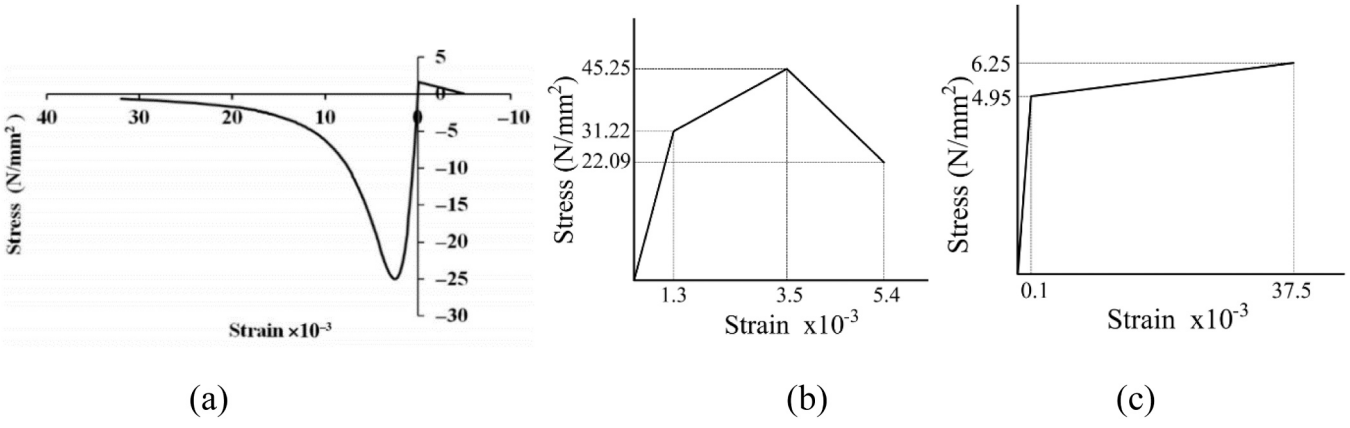

Fig. 4. Stress-strain relationships of (a) NC, (b) ECC under compression, and (c) ECC under tension.

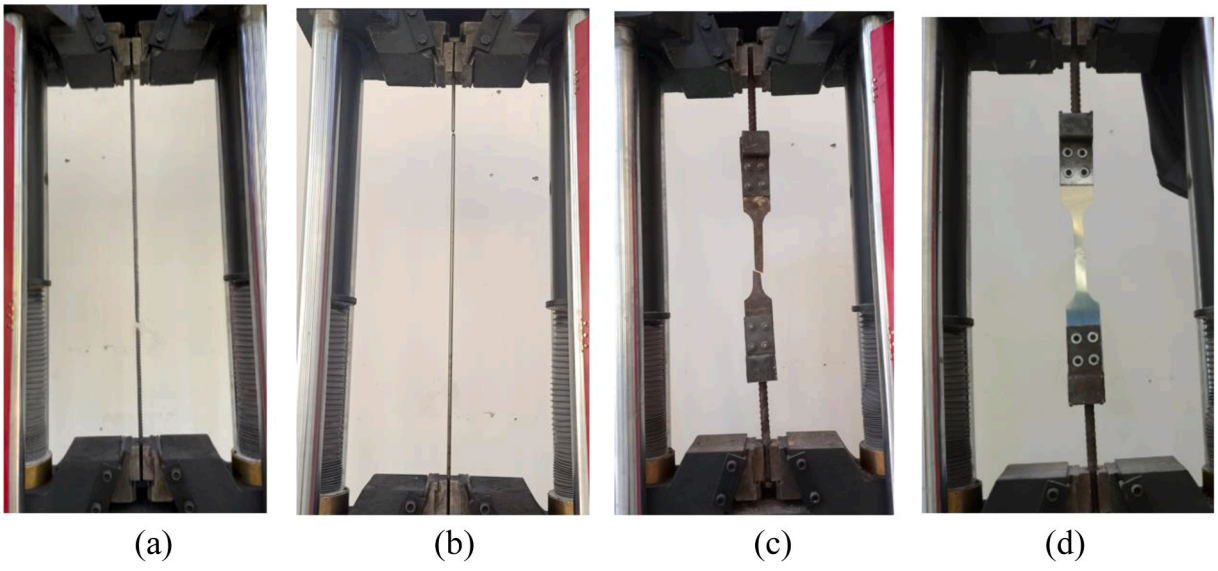

Fig. 5. Tensile coupon testing of (a) steel bar, (b) pre-stressing bar, (c) steel plate, and (d) SSS.

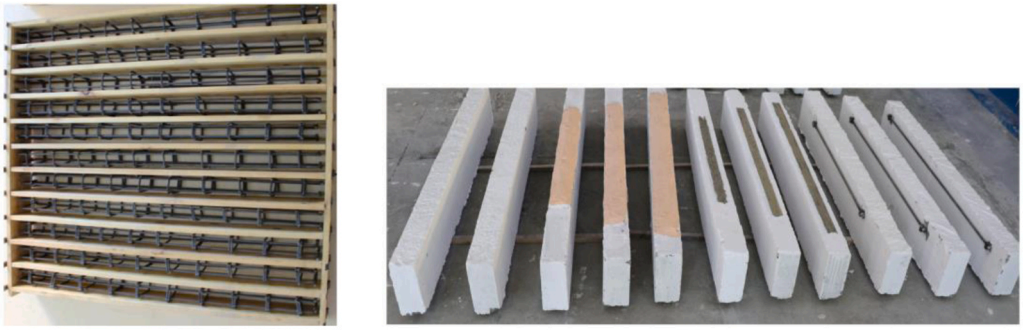

Fig. 7. Preparation of beam specimens (a) formworks, (b) all-prepared beams.

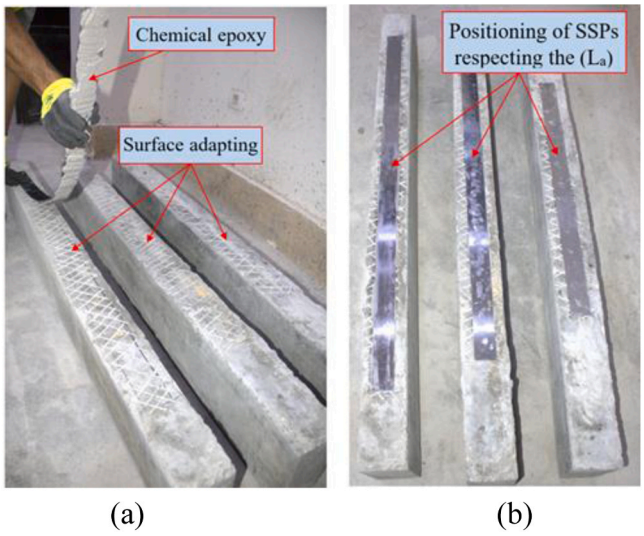

Fig. 8. Strengthening using SSSs: (a) surface adaptation and (b) positioning of SSSs.

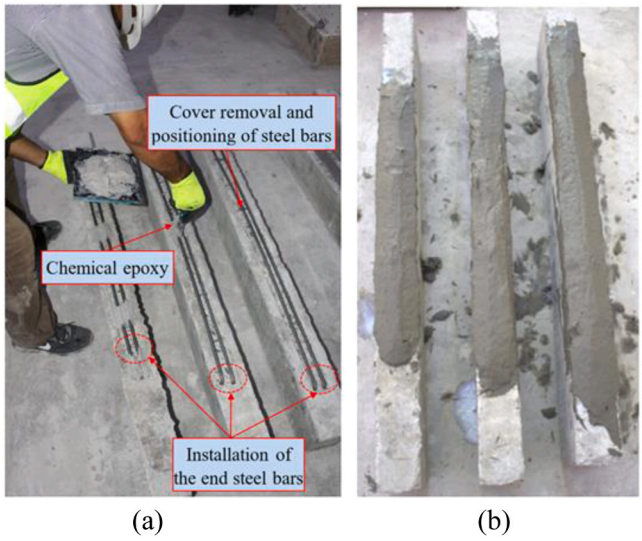

Fig. 9. Strengthening using steel bars at NSM: (a) removal of cover and inserting of additional steel bars, (b) covering the NSM steel bars by ECC.

the control beam, the SSSs-treated beams did not exhibit a significant increase in cracking load, as summarized in Table 2. Subsequently, parallel vertical cracks of varying widths appeared alongside the main crack under tension, as depicted in Fig. 13. These cracks propagated and extended toward the upper surface as the load increased. It is noteworthy that the SSSs beams exhibited more cracks than the defected beam. Furthermore, at higher load levels, inclined cracks, along with the occurrence of a horizontal crack, became evident on the outer surface, as shown in Fig. 13. The presence of this horizontal crack in all failed beams may indicate the initiation of overlapping failure of the main steel bars. It should be noted that the failure predominantly occurred near those cracks. Fig. 13 demonstrates that failure was observed in the overlapping zone of the steel bars resulting in the debonding of the SSSs with a concrete cover separation. The ultimate loads (P_u) of the beams in the SSSs group were enhanced by approximately 40 % to 64 %, as presented in Table 2. Furthermore, the application of SSSs led to a more ductile failure, as illustrated in Fig. 13. Additionally, the SSSs improved the cracking behavior, particularly in terms of the number and width of cracks, when compared to the defected beam.

Group G3 was used to investigate the efficacy of the NSM strengthening technique for beams reinforced with steel bars having insufficient lapped splice length. According to Table 2, the application of strengthening measures delayed the occurrence of the first crack until the load reached 11.23 kN, 12.52 kN, and 12.85 kN, respectively. The cracking loads of B-S-40D, B-S-50D, and B-S-60D increased by 123 %, 148 %, and 155 % respectively, compared to that of the DB beam. The resulting crack pattern closely resembled that of the intact reference beam, as depicted in Fig. 14. As the load increased, the main vertical crack widened. Moreover, a hairline horizontal crack appeared at the interface between the beam's body and the covering ECC layer when the load reached approximately 82 % to 90 % of P_u. Fig. 14 also shows the formation of numerous inclined diagonal cracks. Notably, unlike the SSSs beams, no horizontal cracks occurred in the lapped zone. The presence of additional NSM steel bars prevented this failure mode and improved the beam's performance in the final stage. Ultimately, the beam was unable to withstand any further loads. The ultimate loads of B-S-40D, B-S-50D, and B-S-60D were 30.12 kN, 31.75 kN, and 33.24 kN, respectively, representing improvements of approximately 98 %, 109 %, and 119 % compared to the defected control beam as tabulated in Table 2. The failure mode observed in all tested beams within this group was characterized by pure flexural failure with concrete crushing in the compression zone as illustrated in Fig. 14.

Group G4 was designed to examine the effectiveness of the external prestressing technique. Fig. 15 displays the crack patterns observed in all the beams tested within Group G4. The initial crack emerged at the mid-span at the load values (P_{cr}) of 13.35 kN, 14.92 kN, and 16.25 kN for beams DB-Pr-40D, DB-Pr-50D, and DB-Pr-60D, respectively. This approach significantly prolonged the cracking stage, achieving enhancements of approximately 165 % to 222 % compared to the defected beam as summarized in Table 2. Notably, the prestressing system

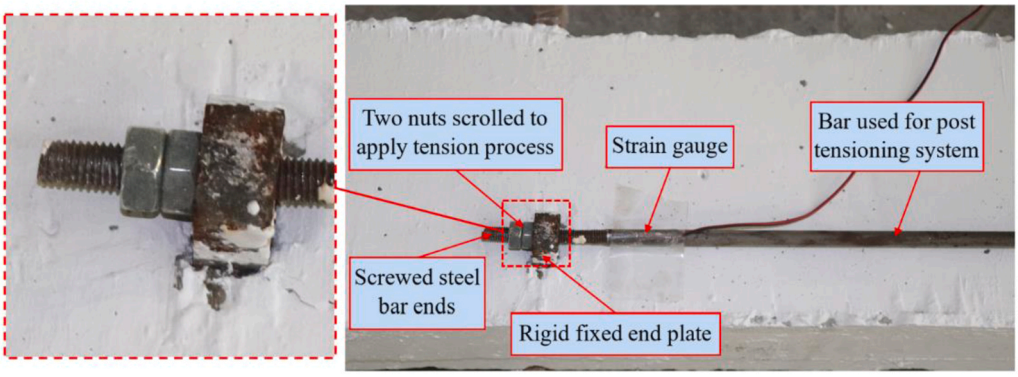

Fig. 10. Strengthening using post-tensioning.

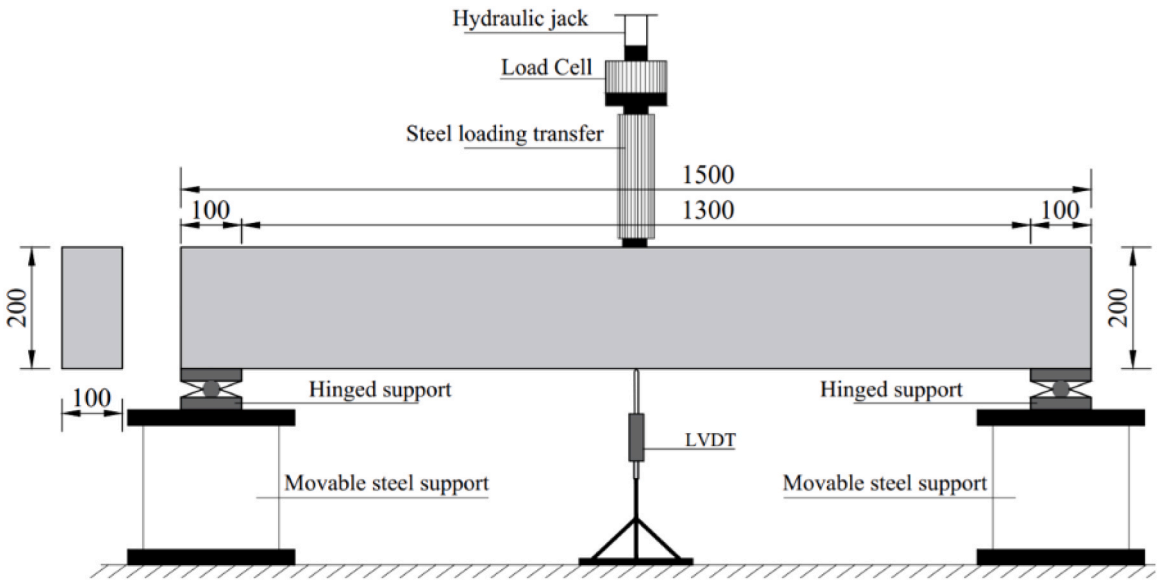

(a) Illustration of test setup

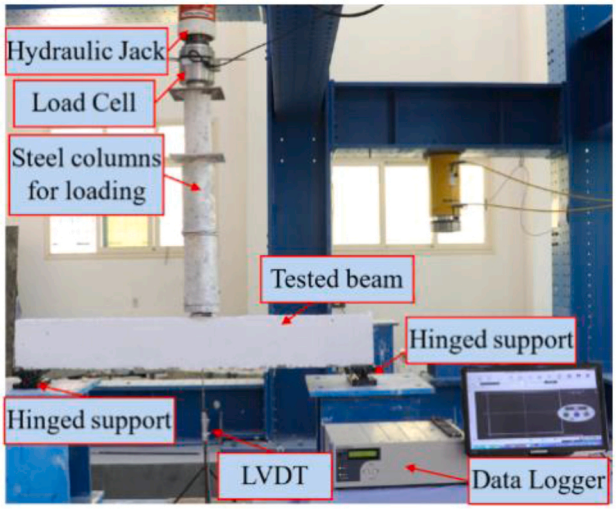

(b) Photo of test setup

Fig. 11. Test set-up.

Table 2
Test results of RC beams.

Group	Specimen	Cracking Stage			Ultimate Stage			K	K_C/K_{DB}	E	Failure mode
		P_{cr} (kN)	$\frac{P_{crB}}{P_{crDB}}$	Δ_{cr} (mm)	P_u (kN)	P_{uB}/P_{uDB}	Δ_{Pu} (mm)				
G1	DB	5.04	1.00	1.77	15.20	1.00	7.54	2.84	1.00	102.43	O
	B0	10.50	2.08	2.31	36.55	2.41	19.51	4.54	1.60	796.25	F
G2	DB	5.04	1.00	1.77	15.20	1.00	7.54	2.84	1.00	102.43	O
	B-SS-40D	7.52	1.49	3.30	21.25	1.40	11.80	2.28	0.80	267.79	F+D
	B-SS-50D	7.86	1.56	2.70	22.86	1.50	12.35	2.91	1.02	258.42	F+D
	B-SS-60D	8.01	1.59	2.38	24.85	1.64	17.14	3.37	1.19	404.19	F+D
G3	DB	5.04	1.00	1.77	15.20	1.00	7.54	2.84	1.00	102.43	O
	B-S-40D	11.23	2.23	3.19	30.12	1.98	22.25	3.52	1.24	644.72	F
	B-S-50D	12.52	2.48	3.43	31.75	2.09	24.11	3.65	1.28	846.95	F
	B-S-60D	12.85	2.55	2.99	33.24	2.19	27.56	4.30	1.51	879.91	F
G4	DB	5.04	1.00	1.77	15.20	1.00	7.54	2.84	1.00	102.43	O
	B-Pr-40D	13.35	2.65	2.70	39.05	2.57	23.85	4.95	1.74	978.58	F
	B- Pr-50D	14.92	2.96	2.84	42.82	2.82	24.53	5.25	1.85	1055.42	F
	B- Pr-60D	16.25	3.22	2.66	47.55	3.13	26.16	6.11	2.15	1002.79	F

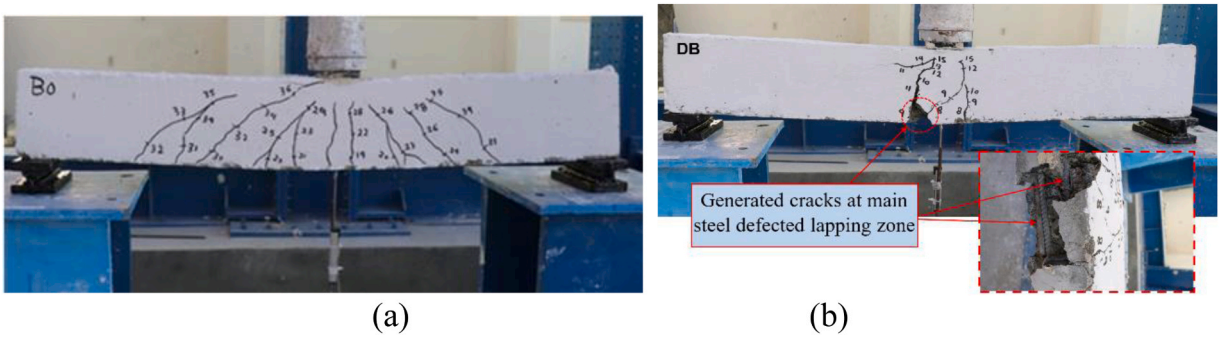

Fig. 12. Failure modes of (a) B0 and (b) DB.

improved the ultimate loads of the beams by 27 % to 54 % higher than that of the beam without strengthening as summarized in Table 2. As the load increased, all the beams exhibited noticeable diagonal cracks propagating towards the upper side, as depicted in Fig. 15. Although horizontal cracks were observed as occurred in the SSSs group, as previously mentioned in overlapping failure, failure did not occur in the same region of the prestressed beams. The ultimate loads (P_u) of the prestressed beams were recorded as 39.05 kN, 42.82 kN, and 47.55 kN, respectively, increasing approximately 157 %, 182 %, and 213 % compared to that of their counterparts in the defected beam.

3.2. Load deflection response and elastic index

Fig. 16 illustrates the load-deflection relationships obtained from tests. Table 2 presents the key experimental findings for all tested reinforced concrete beams at both the cracking and ultimate stages. For the master beam without any defects, the load-deflection response during the initial loading stage demonstrates a linear behavior until reaching a load level ranging between 25–30 % of the ultimate capacity (P_u), as shown in Fig. 16(a). Subsequently, a semi-linear response is observed in the plastic stage, indicating a hardening behavior just prior to reaching the ultimate capacity, followed by pure flexural failure mode. This beam tends to exhibit a trend of variation with elastic, hardening, and softening behavior, depending on the reinforcement ratio and concrete type. The average elastic stiffness of this intact beam is approximately 4.54 kN/mm, as summarized in Table 2, representing an increase of approximately 60 % compared to the defected beam (DB). On the other hand, the defected beam with a 100 mm lap length of reinforcement shows a linear response during the initial loading stage until a deflection of 1.3 mm. As the load increases, hardening behavior is observed, accompanied by failure of the lap splices, as depicted in Fig. 16(a). As expected, the beams strengthened using SSSs exhibit an improved load-deflection performance compared to the defected beam, as shown in Fig. 16(b). The beam with a 40D anchorage length does not show any improvement in the elastic index value. However, the other two EBR beams with L_a of 50D and 60D achieve an increase of 2 % and 19 % in the elastic index, respectively, compared to the defected beam, as summarized in Table 2. The overall load-deflection response is similar to that of the master beam, as depicted in Fig. 16(b). On the other hand, the NSM strengthening strategy didn't result in any improvement in the P_u compared to the control beam. However, the values of the K for all beams tested in this group were 24 % to 51 % higher than the defected control beam, as presented in Table 2. Fig. 16(c) illustrates the load-deflection response for the NSM beams, showing a significant enhancement in both the cracking and ultimate stages compared to the defected beam. This improvement can be attributed to the addition of NSM steel bars. The elastic index increases by approximately 74 %, 85 %, and 115 % for L_a values equal to 40D, 50D, and 60D in the prestressing system, respectively, compared to the defected beam, as summarized in Table 2. Furthermore, the use of different anchorage lengths in the prestressing system, as explored in the fourth group, leads to an increase in both the cracking and ultimate loads, as shown in Fig. 16(d).

3.3. Absorbed energy

Absorbed energy (E) is a crucial factor in determining structural behavior and serves as an important indicator of the efficiency of concrete elements. The E capacity of tested beams can be determined by calculating the area under the load-deflection curves of the tested specimens [50,51]. Table 2 presents the calculated E values for each specimen. It is observed that the application of EBR with SSSs results in a significant improvement in the energy absorption capacity of the tested

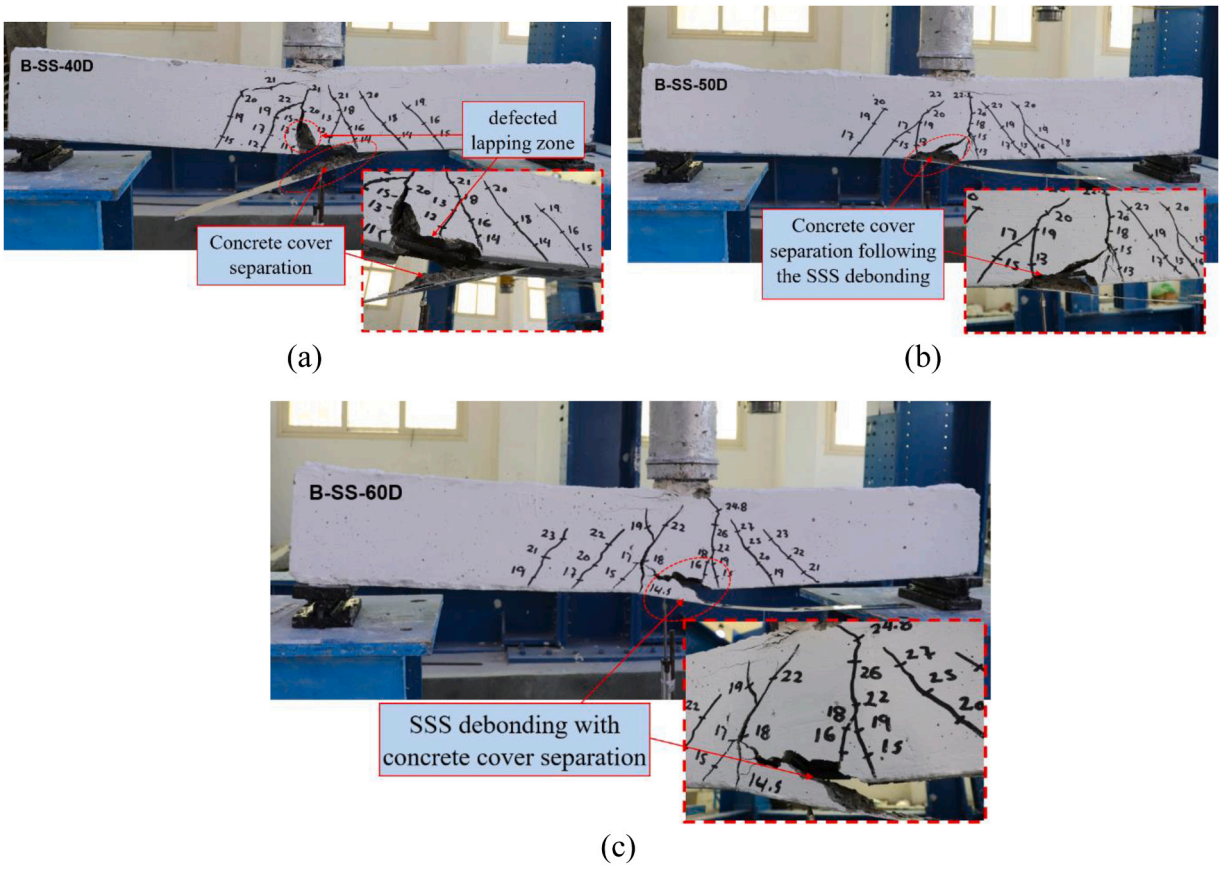

Fig. 13. Failure modes of (a) Beam B-SS-40D, (b) Beam B-SS-50D, and (c) Beam B-SS-60D.

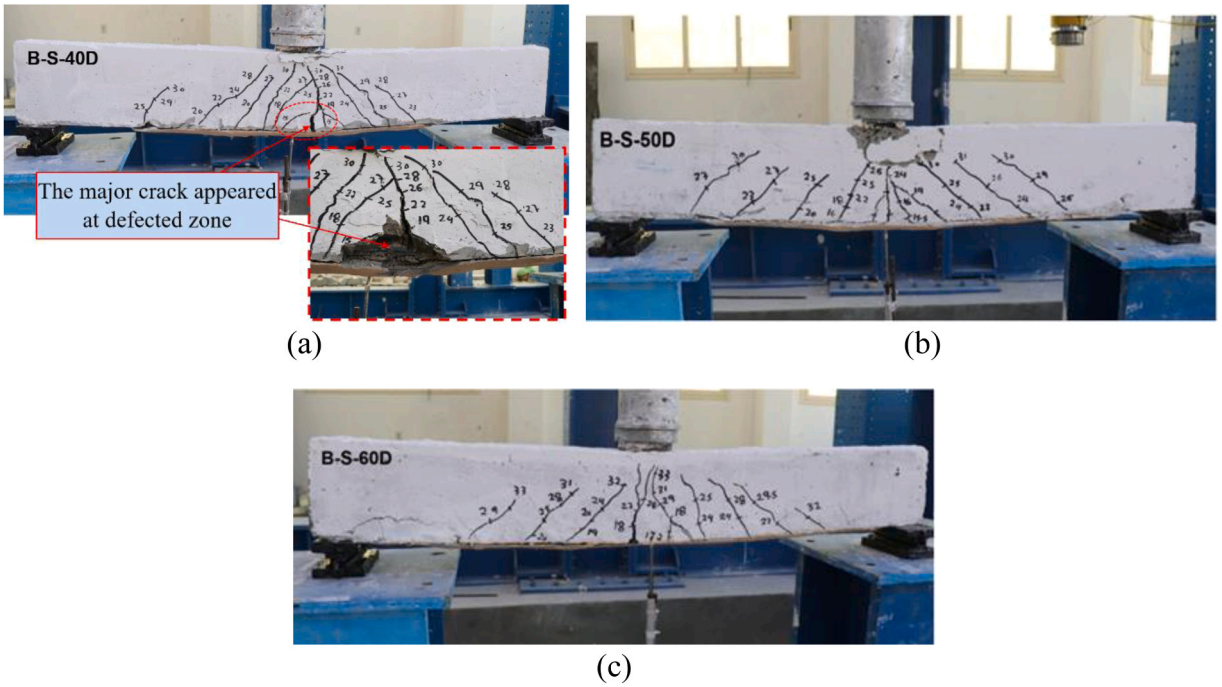

Fig. 14. Failure modes of (a) Beam B-S-40D, (b) Beam B-S-50D, and (c) Beam B-S-60D.

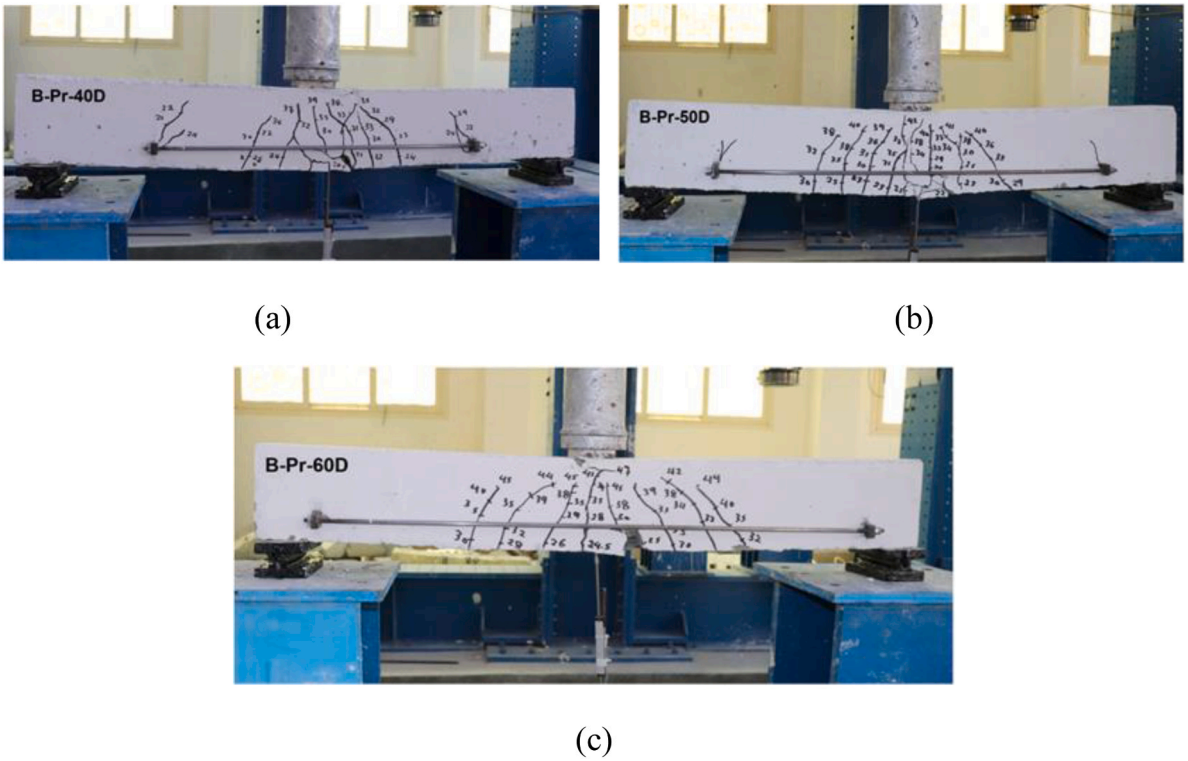

Fig. 15. Failure modes of (a) Beam B-Pr-40D, (b) Beam B- Pr-50D, and (c) Beam B- Pr-60D.

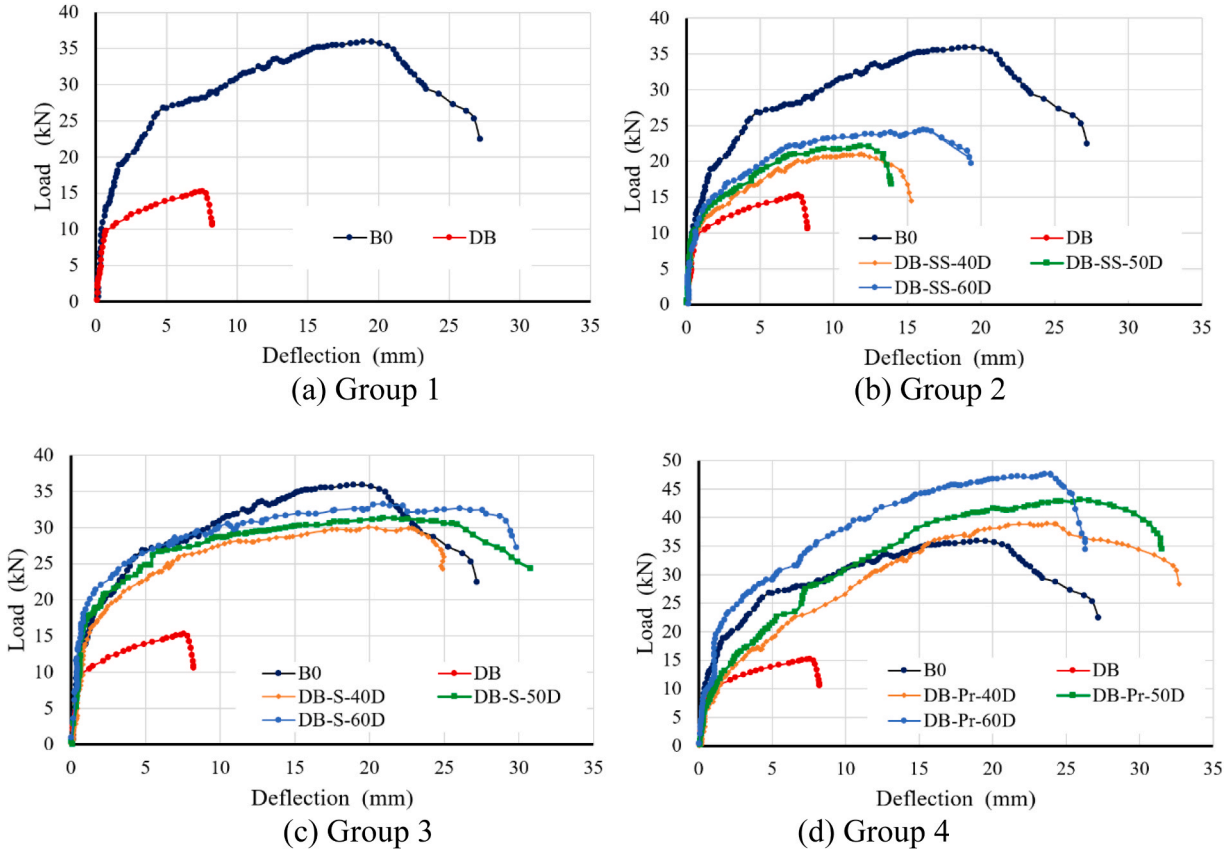

Fig. 16. Load-deflection curves for tested beams.

Table 3
CDP model variables used to model the nonlinear behavior of concrete.

Type	Dilation angle (ψ)	Eccentricity (e)	Shape parameter (K_c)	(f_{bo}/ f_{co})	Viscosity (μ)
NC	30°	0.1	0.667	1.16	0.00001
ECC	35°				

beams, ranging from approximately 2.6 to 3.9 times higher than that of the defected beam. Table 2 clarifies that the *E* values of the beams in Group 3 are approximately 6.2 to 8.5 times higher than that of the defected beam. The prestressing method results in the highest enhancement in *E* value.

4. Numerical simulation

The FE models have been developed using ABAQUS [52] to simulate the responses of strengthened RC beams reinforced with steel bars having insufficient lapped splices.

4.1. Material models

The Concrete Damaged Plasticity model (CDP), available in the materials library in the ABAQUS program was used to simulate the nonlinear behavior of concrete [53,54]. The parameters used to define this model are shown in Table 3 [55]. To define the relationship between stress and strain in both tensile and compression, the results of the direct

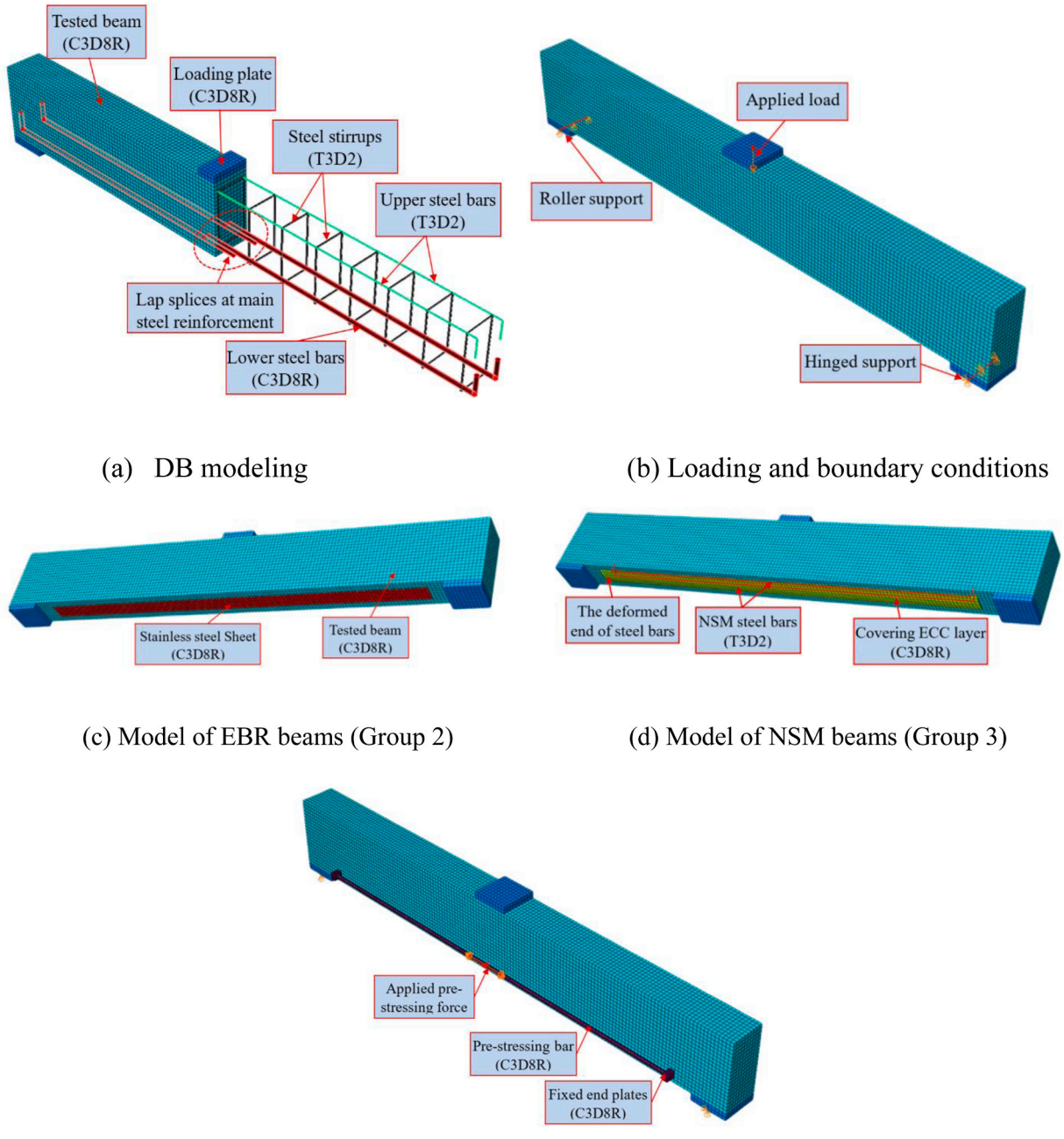

Fig. 17. FE models of strengthened RC beams.

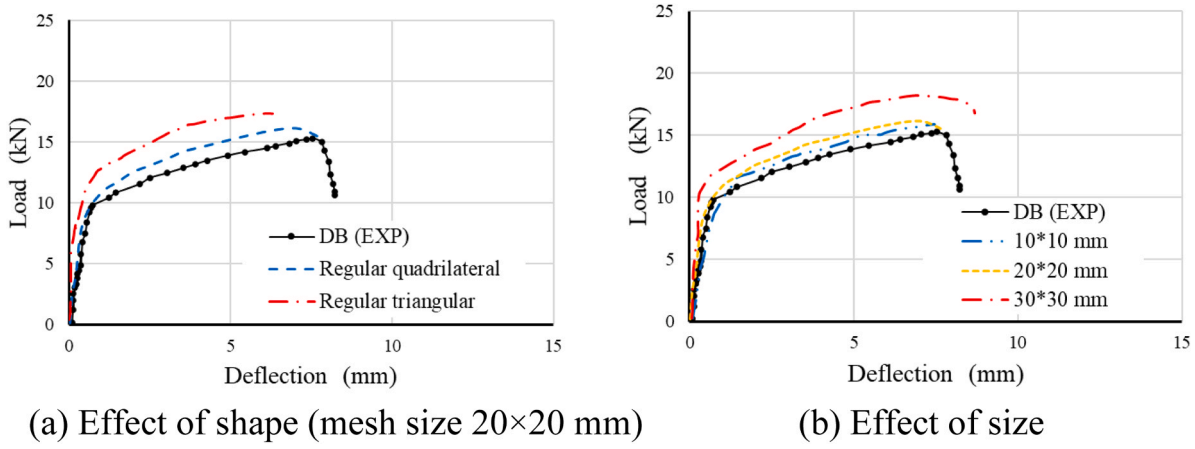

Fig. 18. The effect of the shape and size of the mesh on the load-deflection curve of the beam DB.

compression and tensile tests previously mentioned in Section 2.2 were used, as shown in Fig. 5. The Poisson's ratio of NC and ECC was taken as 0.2 and 0.22, respectively [56].

The actual stress-strain curves obtained from tensile coupon tests were idealized as shown in Fig. 4 to facilitate the material properties required for numerical modeling. The idealization process consisted of four points those were: the initial loading point, the yielding point, the ultimate point, and the failure one [57]. The Poisson's ratio was 0.3 and the modulus of elasticity (E_s) was 2×10^5 N/mm^2.

4.2. Elements, boundary conditions and interactions

C3D8R was used to model concrete beams [58–60], ECC concrete, loading and supporting plates, the steel mechanism used for pre-stressing, the bottom longitudinal reinforcing bars of the beam (connected lower bars) and SSSs, while the element T3D2 was used for the rest of the elements [61,62] including stirrups, the top longitudinal reinforcement bars and strengthening bars.

The interaction between all steel reinforcements and concrete was considered a full bond-embedded region constraint, except that between the lapped splices of rebars and concrete. The model proposed by Gan [63] was used to define the variables of the cohesive interaction between the lapped splices of rebars and concrete in the ABAQUS program. The cohesive interaction was also used to model the interaction between the SSSs and the concrete, as well as the ECC concrete and the beam surface. The values of the variables provided in references [64–66] were adopted to define the variables of this interaction. The entire beam was modeled without taking advantage of symmetry of the beam around the vertical planes. The left support was considered as a roller while the right support was considered as a hinge as shown in Fig. 17(b). For beams subjected to prestressing, the analysis was carried out in two steps. The first step was applying the pretension force to the prestressing bars. This was done by using the bolt load command available in the Abaqus program as shown in Fig. 17(e). The second step was exposing the middle of the load plate with a displacement loading pattern, as shown in Fig. 18.

The sensitivity analyses were conducted on the DB beam to quantify the effect of mesh type, where the following elements were used: C3D8 (an 8-node linear brick element) and C3D6 (a 6-node linear triangular prism element). Fig. 18(a) shows the effect of mesh type on the load-displacement curve. It is clear that the C3D8 can be used to perform numerical study. In addition, the effect of mesh size was studied. For this purpose, the meshes with sizes of 10×10 mm, 20×20 mm, and 30×30 mm were examined. It is clear that the use of a size of 20×20 mm is appropriate when compared to the time consumed to perform the analysis (see Fig. 18(b)).

4.3. Results and validation

Fig. 19 shows a comparison between experimental and numerical load-deflection curves. The figure demonstrates that there is good agreement between them. Table 4 shows the variance between experimental and numerical values of P_{cr}, Δ_{cr}, P_u, and Δ_u, as well as the mean, standard deviation, and coefficient of variation. An excellent match between the test and numerical predictions can be observed. Fig. 20 shows the comparisons of the predicted failure patterns of some of the analyzed beams with the experimental observations. The proposed numerical model was found to capture well the experimental failure patterns. The failure modes include the ductile bending pattern (Beam B0) as shown in Fig. 20(a), the slippage of bars in the lapped splice (Beam DB) as shown in Fig. 20(b), and the debonding of SSSs from the bottom surface of the beam (Beam DB-SS-40D) as shown in Fig. 20(e). The flexural failure mode for beams strengthened with NSM additional steel bars can be seen in Fig. 20(c). Diagonal cracks generated from the two fixed end plates as shown in Fig. 20(d), where the pre-stressing strengthening technique was applied.

5. Parametric study

As explained previously, strengthening with EBSS sheets did not succeed in increasing the capacity of the defective beam DB to reach the capacity of the non-defective beam B0. The capacity of beam B-SS-60D barely reached 68 % of the capacity of beam B0. This method of strengthening also did not succeed in changing the failure pattern to the preferred flexural pattern, as the three beams B-SS-40D, B-SS-50D, and B-SS-60D collapsed due to the debonding of the sheets. This collapse pattern is brittle and unfavorable. The collapse by debonding is due to the use of sheets that have a small bond area with the bottom surface of the concrete beam. Sheets with a width of 50 mm were used, even though the total width of the beam is 100 mm, and no end anchors were used.

To address this shortcoming, the FE model developed was employed to study the behavior of RC beams with insufficient lapped splice length of reinforcement strengthened by EBSS sheets. The EBSS sheets with a width of 100 mm and a thickness of 1.57 mm were used. Four beams were studied, which were B-ESS-40D, B-ESS-50D, B-ESS-60D, and B-ESS-65D. The lengths of EBSS sheets were 800 mm, 1000 mm, 1200 mm, and 1300 mm. Two beams B-ESS-40D-A and B-ESS-50D-A were simulated to assess the effects of end anchors as shown in Fig. 21. The portion of the screw penetrating the concrete was modeled as a full bond-tie constraint, while the hard contact allowing separation with a penalty friction coefficient of 0.44 was relied upon to connect the opposite surfaces of the steel screw and the SSS [48,67,68].

Fig. 22 shows the load-displacement curves of the analyzed beams. It

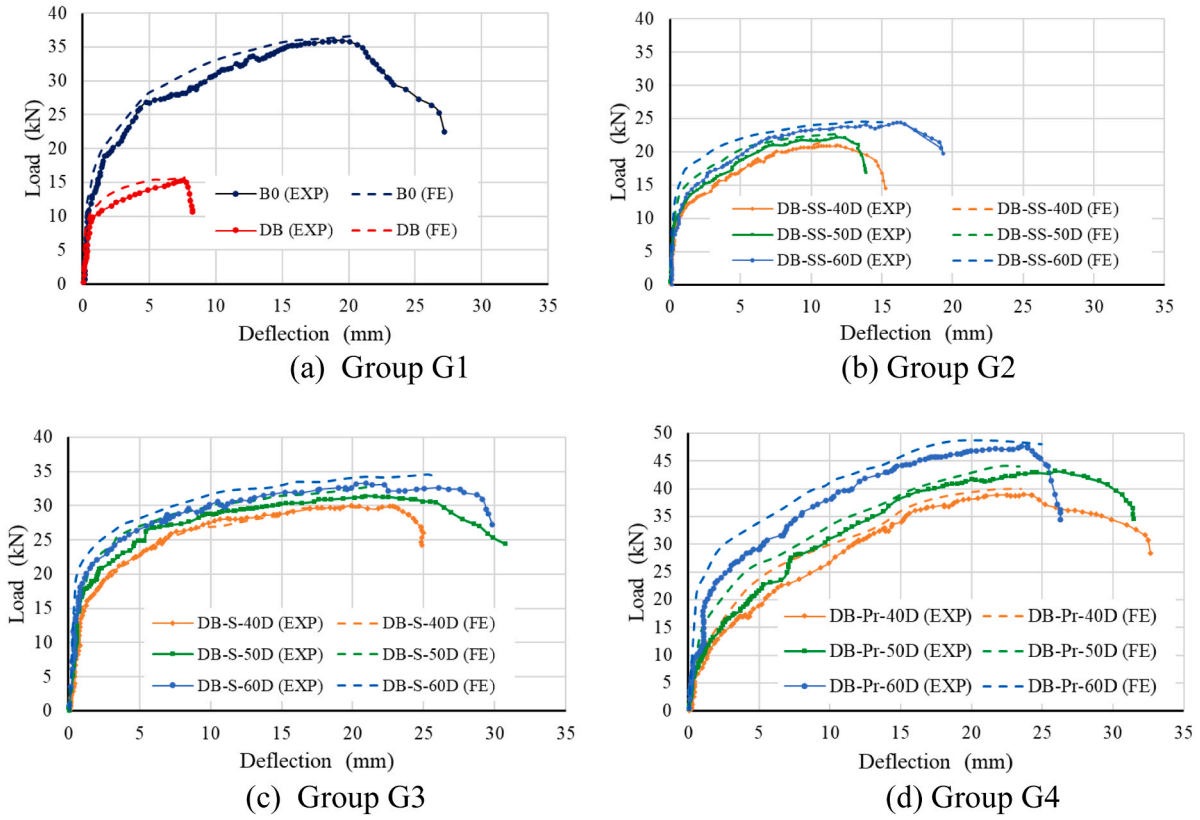

Fig. 19. Comparison of predicted and experimental load-displacement curves.

can be seen from Fig. 22(a) that increasing the length of EBSS sheet increases the ultimate load of strengthened RC beams. The ultimate loads of beams B-ESS-40D, B-ESS-50D, B-ESS-60D, and B-ESS-65D are 32.98 kN, 39.80 kN, 45.02 kN, 47.90 kN, respectively. The ultimate load of these beams increases by 111 %, 155 %, 189 %, 207 %, respectively when compared with that of defected beam DB. They represent 0.90, 1.09, 1.23, and 1.31 times the ultimate load of the non-defected beam B0, respectively. Beams B-ESS-40D, B-ESS-50D and B-ESS-60D collapsed by totally debonding of SSSs (see Fig. 23(a)), while beam B-ESS-65D collapsed by flexure with partial debonding occurring in the area between the ends of the sheet (see Fig. 23(b)).

The load-displacement curves for beams B-ESS-40D-A and B-ESS-50D-A with anchors are provided in Fig. 22(b). The ultimate load of beam B-ESS-40D-A is 45.40 kN, which increases by 191 % compared to that of DB beam and 124 % compared to that of B0 beam. The beam B-ESS-40D-A collapsed by debonding between the anchors, with bearing failure of sheet around the anchor holes as shown in Fig. 23(c). The ultimate load of the beam B-ESS-50D-A increases by 208 % when compared with that of beam DB and 131 % when compared with that of beam B0. The failure mode of B-ESS-50D-A is flexural which is ductile. (see Fig. 23(d)).

It can be concluded that strengthening RC beams with insufficient lapped splice length of reinforcing bars using EBSS sheets over the entire clear span of the beams significantly improves their load-carrying capacities and ductility. It is suggested that when shorter EBSS sheets are used, the end of sheet should be anchored by anchors.

6. Analytical model

The sectional analysis of a strengthened RC beam with insufficient lapped splice length of reinforcing bars is undertaken to determine its ultimate moment capacity, thereby the load-carrying capacity of the beam can be computed. Fig. 24 shows the beam cross-section at its mid-span, distribution of strains, stresses and resultant forces in the section for a beam strengthened by NSM. It is assumed that at the ultimate limit state, the strain of the additional reinforcing bars embedded within the ECC layer reaches or exceeds the yield strain ($\varepsilon_{s,add} \geq \varepsilon_y$), and the compressive strains of the top fibers reaches the ultimate strain of the concrete ($\varepsilon_c = \varepsilon_{cu}$).

The force equilibrium condition can be expressed as:

$$C_c + C_s' = T_{s,add} + T_{ECC} + T_s \tag{1}$$

where C_c and C_s' are the compressive forces in the concrete and the top steel; $T_{s,add}$,T_{ECC}, and T_s are the tensile forces in the additional steel embedded within the ECC layer, the ECC layer itself, and the bottom steel, respectively.

Eq. (1) can be rewritten as:

$$0.85 f_c' \lambda c \quad b \quad + A_s' f_s' = A_{s,add} f_y + A_{ECC} f_{tu,ECC} + A_s f_s \tag{2}$$

where f_s' and f_s can be obtained from the following equations:

$$f_s' = \begin{cases} \varepsilon_{cu} \quad \dfrac{(c-d')}{c} E_s \, if \, \varepsilon_s' \quad < \quad \varepsilon_y \\ f_s' = \quad f_y \, if \, \varepsilon_s' \quad \geq \quad \varepsilon_y \end{cases} \tag{3}$$

$$f_s = \begin{cases} \varepsilon_{cu} \quad \dfrac{(d-c)}{c} E_s \leq f_y \, if \, q_b \leq \quad q_{bu} \\ f_s = \quad 0 \, if \, q_b > \quad q_{bu} \end{cases} \tag{4}$$

where,

$$q_b = \frac{f_s}{4} \frac{d_b}{l_s} \tag{5}$$

$$q_{bu} = (1.2 + 3\frac{c'}{d_b} + 50\frac{d_b}{l_s} + k_{tr}')\sqrt{f_c'} \& k_{tr}' = \frac{A_{tr}}{500} \frac{f_{yt}}{s} \frac{}{d_b} \leq 3.0 \tag{6}$$

Table 4
Validation of the finite element analysis results.

Specimen ID	P_{cr} (kN)			Δ_{cr} (mm)			P_u (kN)			Δ_u (mm)		
	EXP.	FE	FE/ EXP	EXP.	FE	FE/ EXP	EXP	FE	FE/ EXP	EXP	FE	FE/ EXP
DB	5.04	5.15	1.02	1.77	1.72	0.97	15.2	15.56	1.02	7.54	7.45	0.99
B0	10.5	10.89	1.04	2.31	2.28	0.99	36.55	37.25	1.02	19.51	18.95	0.97
B-SS-40D	7.52	7.78	1.03	3.3	3.21	0.97	21.25	22.01	1.04	11.8	11.63	0.99
B-SS-50D	7.86	7.98	1.02	2.7	2.65	0.98	22.86	23.5	1.03	12.35	12.15	0.98
B-SS-60D	8.01	8.2	1.02	2.38	2.32	0.97	24.85	25.63	1.03	17.14	16.85	0.98
B-S-40D	11.23	11.52	1.03	3.19	3.12	0.98	30.12	31.25	1.04	22.25	21.65	0.97
B-S-50D	12.52	12.85	1.03	3.43	3.35	0.98	31.75	32.25	1.02	24.11	23.55	0.98
B-S-60D	12.85	13.24	1.03	2.99	2.89	0.97	33.24	34.36	1.03	27.56	27.12	0.98
B-Pr-40D	13.35	13.65	1.02	2.7	2.65	0.98	39.05	40.53	1.04	23.85	23.25	0.97
B- Pr-50D	14.92	15.36	1.03	2.84	2.77	0.98	42.82	43.55	1.02	24.53	24.11	0.98
B- Pr-60D	16.25	16.81	1.03	2.66	2.63	0.99	47.55	48.62	1.02	26.16	25.57	0.98
Avg			1.03			0.98			1.03			0.98
SD			0.007			0.007			0.008			0.006
CoV			0.007			0.007			0.008			0.006

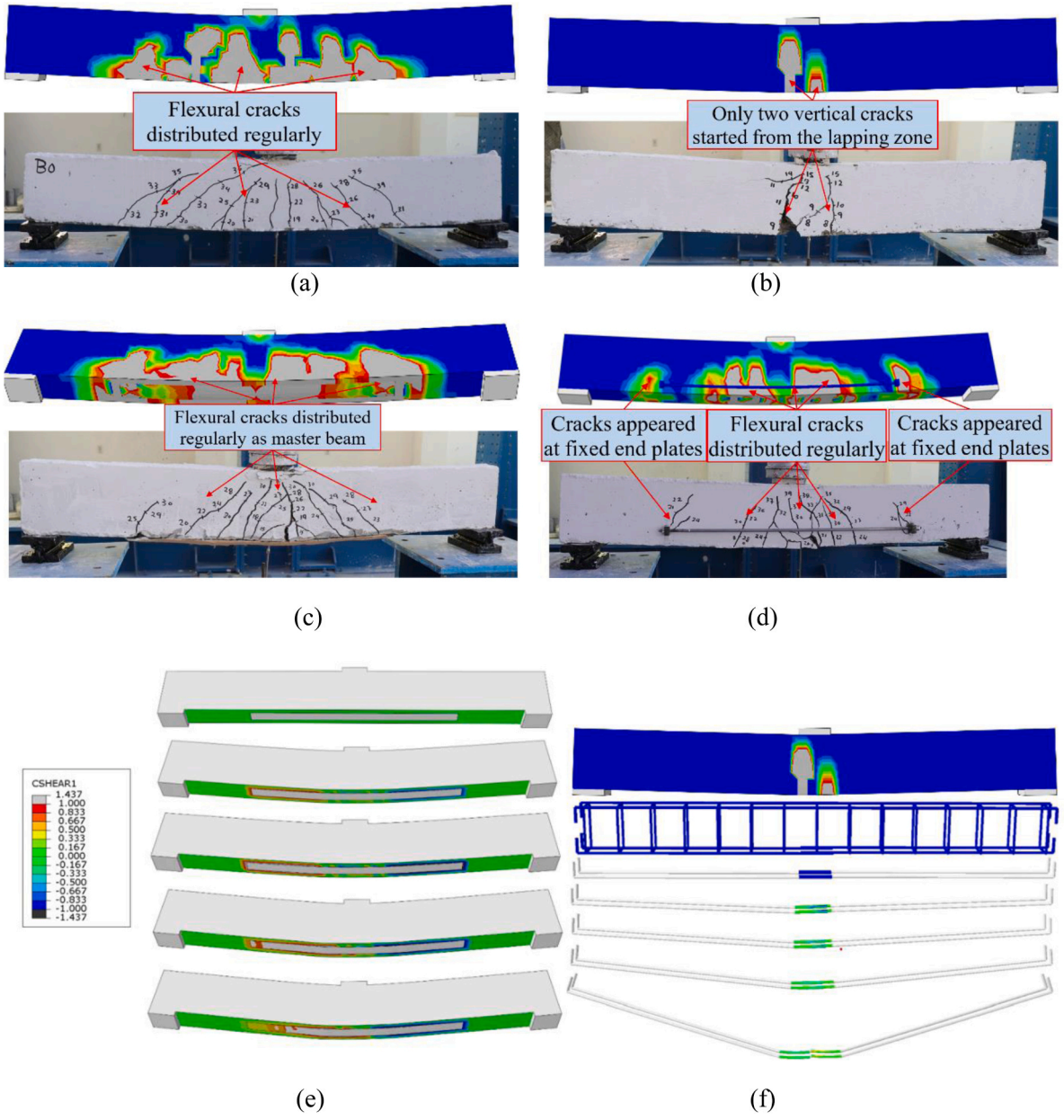

Fig. 20. Numerical failure patterns: (a) Beam B0, (b) Beam DB, (c) Beam DB-S-40D, (D) Beam DB-Pr-40D, (e) SSSs beams, and (f) Slippage of bars in the lap splice.

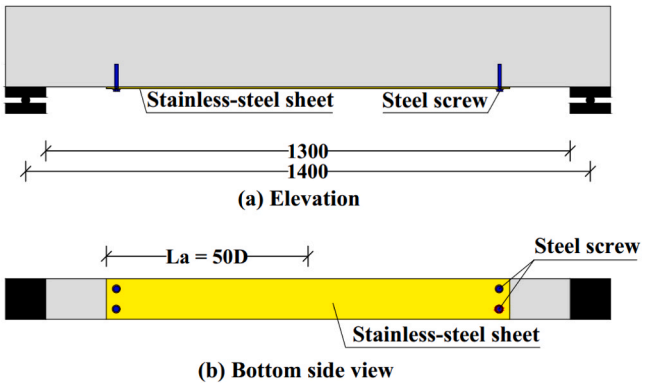

Fig. 21. Beams strengthened by stainless-steel sheets bonded with epoxy adhesive and steel screws. (Units: mm).

where: f_c' is the concrete compressive strength, λ is the ratio between the length of the base of the rectangle equivalent to the compressive stresses to the length of the base of the true stresses and is equal to 0.8 according to EN1992–1-1 [69], c is the neutral axis depth, b is the width of beam section, A_s' is the area of the reinforcement on the compression side, f_s' is the stress of the reinforcement in the compression side, $A_{s,add}$ is the area of the reinforcement embedded within the ECC layer, f_y is the yield stress of the reinforcement embedded within the ECC layer, A_{ECC} is the area of the ECC layer, $f_{tu,ECC}$ is the tensile strength of ECC, A_s is the area of the splice reinforcement, f_s is the stress of the splice reinforcement, q_b is the bond stress around the splice reinforcement, q_{bu} is the bond strength of concrete around the splice reinforcement, d_b is the diameter of the splice reinforcement bars, l_s is the splice length, c' is smaller of clear side cover, bottom cover or half the clear spacing between bars, k_{tr}' is steel confinement index (k_{tr}'= 0 for no transverse reinforcement), A_{tr} is the cross-sectional area of transverse reinforcement within spacing s and crossing the plane of splitting, s is the spacing of transverse reinforcement within the splice zone, d' is the concrete cover for compression steel, d is the original effective depth of the beam section, d_1 is the new effective depth of the beam section.

The neutral axis depth can be obtained from Eq. (2). The ultimate moment capacity of the section ($M_{u\ an.}$) can be determined by taking moments about the action line of C_c as follows:

$$M_{uan.} = C_s' \left(\frac{\lambda c}{2} - d' \right) + (T_{s,add} + T_{ECC})\left(d_1 - \frac{\lambda c}{2}\right) + T_s\left(d - \frac{\lambda c}{2}\right) \tag{7}$$

Fig. 25 shows a cross-section of one of the beams strengthened using the post-tensioned bar technique. From this, it can be noted that Eqs. (2) and (7) respectively become as follows:

$$0.85\ f_c'\lambda c\ b + A_s'f_s' = T_{Prt} + A_sf_s \tag{8}$$

$$M_{uan.} = C_s' \left(\frac{\lambda c}{2} - d' \right) + T_{Prt}\left(d_{Pr} - \frac{\lambda c}{2}\right) + T_s\left(d - \frac{\lambda c}{2}\right) \tag{9}$$

where T_{Prt} is the total tensile force in the bars at the ultimate loading stage, calculated using the following equation:

$$T_{Prt} = P_{Pr} + A_{Prt}E_{Pr}\varepsilon_{cu}\frac{(d_{Pr} - c)}{c} \le A_{Prt}\ f_{y,Pr} \tag{10}$$

where P_{Pr} is the total initial tensile force of the bars assuming no losses, A_{Prt} is the total area of the bars, E_{Pr} is the modulus of elasticity of the bar material, d_{Pr} is the depth to which the bars are located, measured from the fibers of the upper section in the compression direction, and $f_{y,Pr}$ is the yield stress of the bar material.

Fig. 26 shows the cross-section of one of the beams strengthened by SSSs. From this, it is clear that Eqs. (2) and (7) become as follows:

$$0.85f_c'\lambda c\ b + A_s'f_s' = A_{ss}f_{y,ss} + A_sf_s \tag{11}$$

$$M_{uan.} = C_s' \left(\frac{\lambda c}{2} - d' \right) + T_{ss}\left(d_{ss} - \frac{\lambda c}{2}\right) + T_s\left(d - \frac{\lambda c}{2}\right) \tag{12}$$

where A_{ss}, $f_{y,ss}$, T_{ss}, and d_{ss} are the area, yield stress, tensile force, and effective depth of the SSS, respectively.

The ultimate load $P_{u\ an.}$ of the beam can be determined by:

$$P_{uan.} = \frac{4\ M_{uan.}}{L} \tag{13}$$

where L is the effective span of the beam.

To ensure the validity of the proposed analytical model, the maximum load obtained analytically ($P_{u\ an.}$) is compared to the maximum load obtained numerically ($P_{u\ num.}$). The ultimate loads obtained are given in Table 5. It appears that the proposed analytical model accurately computes the ultimate capacity of RC beams strengthened to resist insufficient lapped splice length of reinforcing bars. The mean ratio of $P_{u\ an.}$ / $P_{u\ num.}$ is 0.98 with SD of 0.0147 and CoV of 0.015.

7. Conclusions

This paper has presented an experimental study and finite element modeling of strengthened RC beams containing insufficient lapped

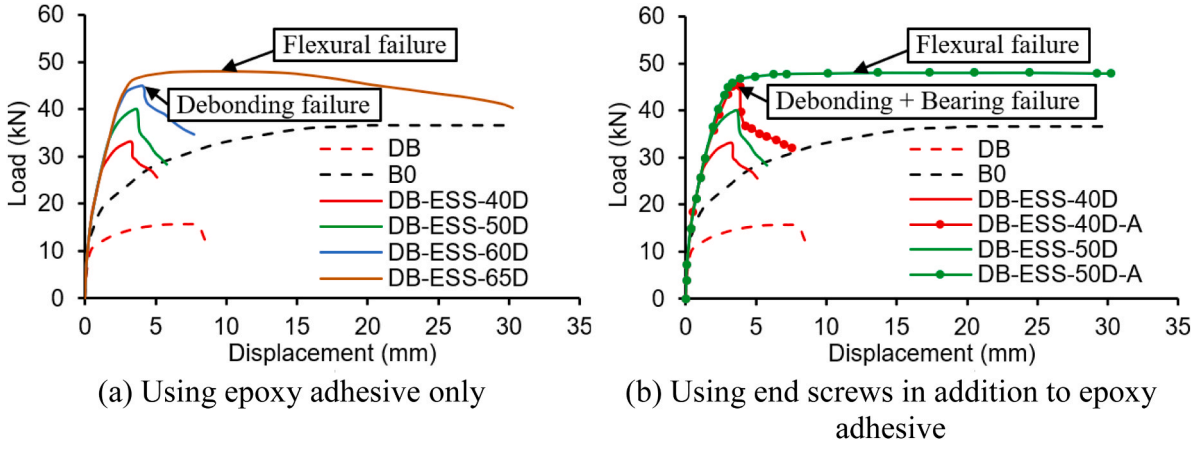

Fig. 22. Numerical load-displacement curves for parametric study beams.

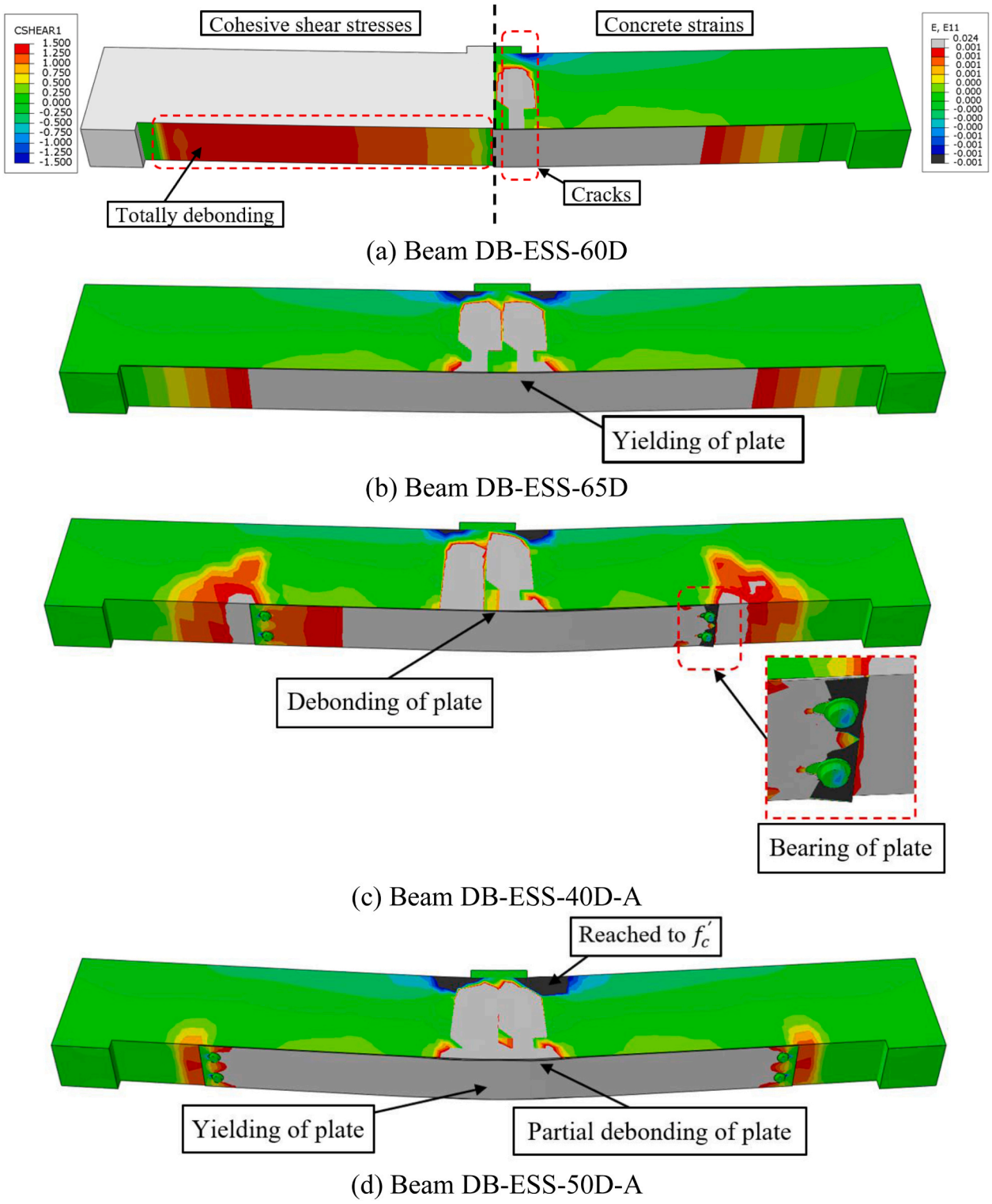

Fig. 23. Numerical failure patterns of parametric study beams.

splice length of longitudinal reinforcing bars. Test results have been reported on the defected RC beams, which were strengthened by using the externally bonded stainless-steel (EBSS) sheets, the near surface mounted (NSM) steel bars, and the external prestressing method. The effects of the strengthening methods and anchorage lengths on the structural behavior have been quantified. The FE modeling of strengthened RC beams has been developed and verified by test results presented in this paper. The following conclusions are drawn from this study:

(a) The ultimate load of the defected beams strengthened by EBSS sheets with an anchorage length of 400 mm, 500 mm, and 600 mm is 40 %, 50 %, and 64 % higher than that of the control defected beam (DB), respectively. Attaching a EBSS sheet of 1200-mm length to the RC beam increases its elastic index and

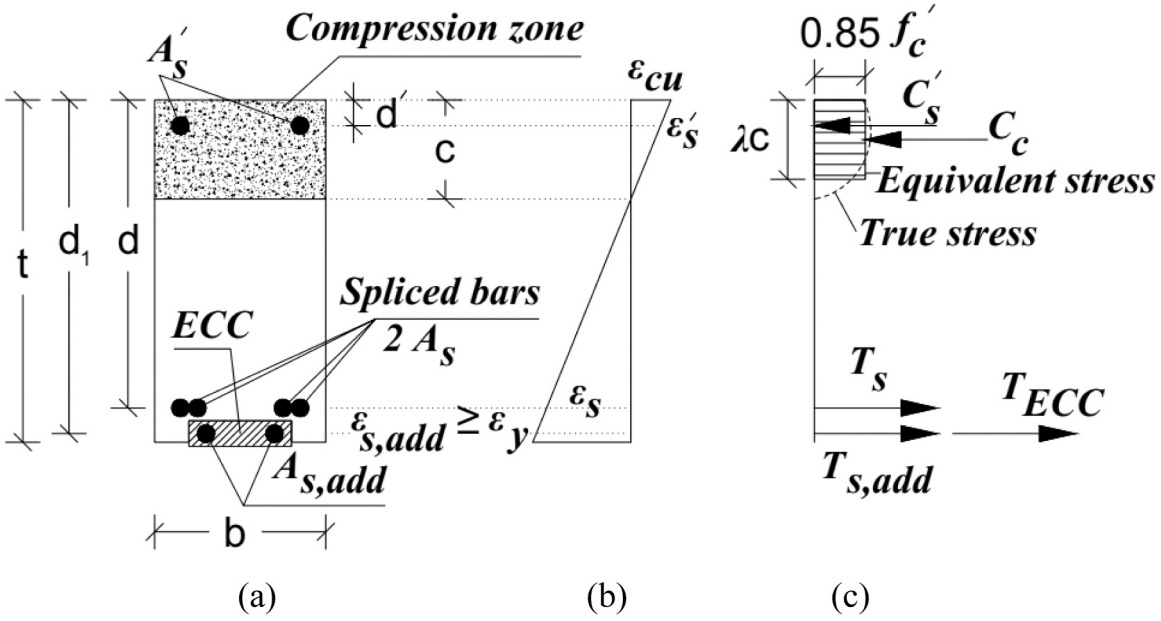

Fig. 24. Details of the beam section, strains, stresses and forces.

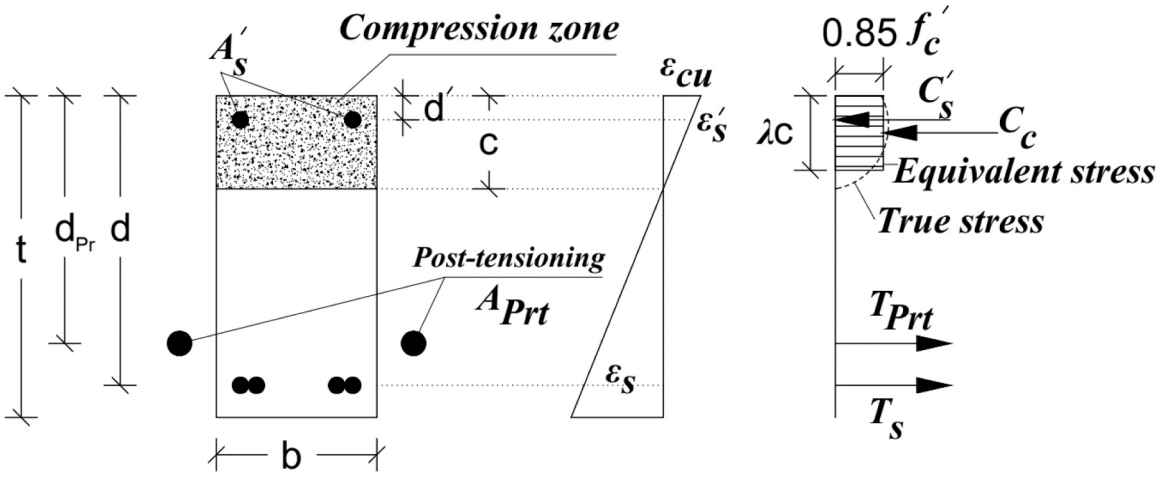

Fig. 25. Cross-section of a beam strengthened using post-tensioned bars.

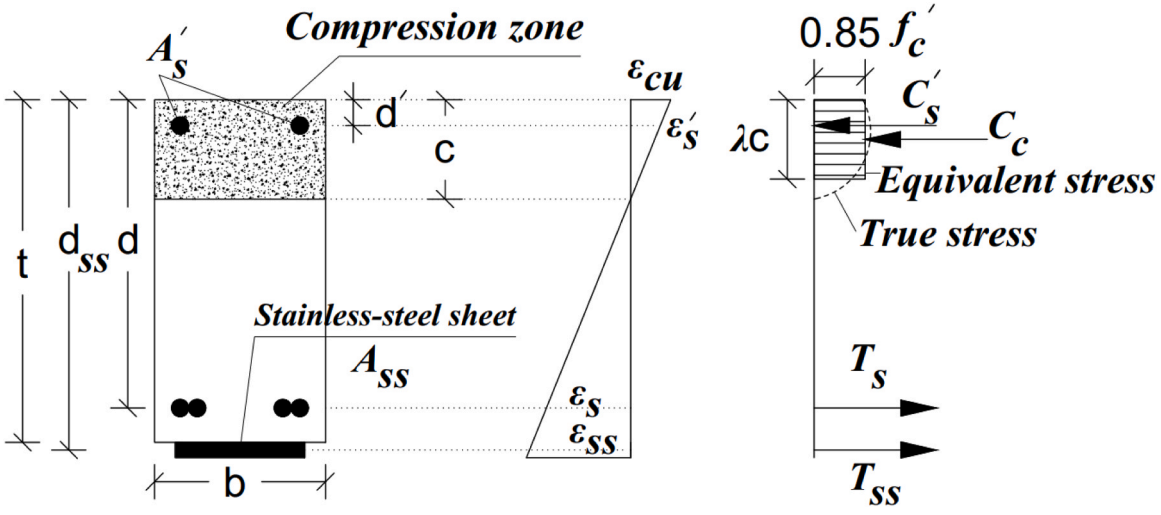

Fig. 26. Cross-section of a beam strengthened by external SSSs.

Table 5
Comparison of the ultimate capacity analytically and numerically.

Beam	$P_{u\ an.}$ (kN)	$P_{u\ num.}$ (kN)	$P_{u\ an.}$ / $P_{u\ num.}$
B-ESS-50D-A-(A_{SS}=157 mm^2)	46.34	47.92	0.97
B-ESS-50D-A-(A_{SS}=235 mm^2)	66.31	68.50	0.97
B-ESS-50D-A-(A_{SS}=314 mm^2)	88.21	89.80	0.98
DB-S-50D-($A_{S,add}$=2Φ6)	13.85	14.25	0.97
DB-S-50D-($A_{S,add}$=2Φ8)	21.34	21.74	0.98
DB-S-50D-($A_{S,add}$=2Φ10)	31.15	32.25	0.97
DB-S-50D-($A_{S,add}$=2Φ12)	45.95	46.54	0.99
B- Pr-60D-(P_{Pr}=10.5 kN)	49.35	48.62	1.02
B- Pr-60D-(P_{Pr}=21.0 kN)	54.73	55.70	0.98
B- Pr-60D-(P_{Pr}=31.5 kN)	61.78	62.59	0.99
Avg			0.98
SD			0.0147
CoV			0.015

absorbed energy by 19 % and 29 %, respectively, when compared with the control defected beam.

(b) Strengthening the RC beams by NSM steel bars with an anchorage length of 40D, 50D, and 60D increases the ultimate load of the beams by 98 %, 109 %, and 119 %, respectively when compared with the control defected beam.

(c) The ultimate load of the strengthened RC beams increases with an increase in the length of the prestressing steel bars. It is recommended that the anchorage length of the prestressing steel bars should be greater than 40D. The elastic stiffness of strengthened beams with prestressing bars of an anchorage length of 40D, 50D, and 60D is 74 %, 85 %, and 115 % higher than that of the control beam.

(d) The developed FE model can accurately simulate the stiffness and strength performance of strengthened concrete beams reinforced by longitudinal steel bars with insufficient lapped splice lengths.

(e) Strengthening RC beams with insufficient lapped splice length of reinforcement using EBSS sheets over the entire clear span of the beams significantly improves their load-carrying capacities and ductility. This method increased the capacity of beam B-ESS-65D by 207 % when compared with that of the control beam. It is suggested that when shorter EBSS sheets are used, the end of sheet should be anchored by anchors.

(f) For strengthened beams, the proposed analytical model can estimate the ultimate load with good accuracy.

CRediT authorship contribution statement

Mohamed Ghalla: Writing – original draft, Visualization, Project administration, Methodology, Investigation, Funding acquisition, Formal analysis, Data curation, Conceptualization. **Mizan Ahmed:** Writing – review & editing, Visualization. **Qing Quan Liang:** Writing – review & editing, Visualization. **Moataz Badawi:** Writing – review & editing, Visualization, Methodology, Investigation. **Galal Elsamak:** Writing – review & editing, Visualization, Validation, Software, Formal analysis. **Mohamed A. El Zareef:** Writing – review & editing, Visualization, Methodology, Investigation, Funding acquisition.

Declaration of Competing Interest

The authors declare that they have no known competing financial interests or personal relationships that could have appeared to influence the work reported in this paper.

Data availability

Data will be made available on request.

References

[1] Dabiri H, Kheyroddin A, Dall'Asta A. Splice methods used for reinforcement steel bars: a state-of-the-art review. Constr Build Mater 2022;320:126198.
[2] Hamad BS, Harajli MH, Jumaa G. Effect of fiber reinforcement on bond strength of tension lap splices in high-strength concrete. Acids Struct J 2001;98:638–47.
[3] Gilbert R, Kilpatrick A. The strength and ductility of lapped splices of reinforcing bars in tension. Aust J Struct Eng 2015;16:35–46.
[4] Lee J-K. Bonding behavior of lap-spliced reinforcing bars embedded in ultra-high strength concrete with steel fibers. KSCE J Civ Eng 2016;20:273–81.
[5] Rakhshanimehr M, Esfahani MR, Kianoush MR, Mohammadzadeh BA, Mousavi SR. Flexural ductility of reinforced concrete beams with lap-spliced bars. Can J Civ Eng 2014;41:594–604.
[6] AS 3600. Concrete structures. Standards Australia, Sydney, NSW, Australia; 2018.
[7] ACI 318–19. Building code requirements for structural concrete and commentary. Farmington Hills, Michigan, USA; 2019.
[8] Akın SK, Kartal S, Müsevitoğlu A, Sancıoğlu S, Zia AJ, Ilgün A. Macro and micro polypropylene fiber effect on reinforced concrete beams with insufficient lap splice length. Case Stud Constr Mater 2022;16:e01005.
[9] Al-Mamory ZK, Al-Ahmed AHA. Behavior of steel fiber reinforced concrete beams with CFRP wrapped lap splice bars. Structures 2022;44:1995–2011.
[10] Askar HS, Mohamed AH, Tahwia AM, El-Demerdash WE. An experimental investigation on the characteristics of tension lap splice in UHPFRC beams. Innov Infrastruct Solut 2023;8:130.
[11] Juntanalikit P, Jirawattanasomkul T, Pimanmas A. Experimental and numerical study of strengthening non-ductile RC columns with and without lap splice by carbon fiber reinforced polymer (CFRP) jacketing. Eng Struct 2016;125:400–18.
[12] Garcia R, Helal Y, Pilakoutas K, Guadagnini M. Bond behaviour of substandard splices in RC beams externally confined with CFRP. Constr Build Mater 2014;50:340–51.
[13] Hamoda A, El-Mandouh MA, Ahmed M, Abadel AA, Liang QQ, Elsamak G. Experimental and numerical studies of reinforced concrete stair beams strengthened with steel bars and plates. Eng Struct 2023;297:117037.
[14] El-Mandouh MA, Elsamak G, Rageh BO, Hamoda A, Abdelazeem F. Experimental and numerical investigation of one-way reinforced concrete slabs using various strengthening systems. Case Stud Constr Mater 2023;18:e01691.
[15] El-Mandouh MA, Hu JW, Shim WS, Abdelazeem F, ELsamak G. Torsional improvement of RC beams using various strengthening systems. Buildings 2022;12:1776.
[16] Mansour W, Li W, Ghalla M, Badawi M, El Zareef MA. Improving the punching capacity of two-way RC flat slabs via external strengthening using various configurations of aluminum sheets. Constr Build Mater 2024;420:135611.
[17] Elsamak G, Fayed S. Flexural strengthening of RC beams using externally bonded aluminum plates: an experimental and numerical study. Adv Concr Constr 2021;11:481–92.
[18] Mostofinejad D, Moghaddas A. Bond efficiency of EBR and EBROG methods in different flexural failure mechanisms of FRP strengthened RC beams. Constr Build Mater 2014;54:605–14.
[19] Jin Y-H, Zhou Z-Y, Bao B-L, Wang H-Y, Wang T. Experimental study on the seismic performance of clay brick masonry wall strengthened with stainless steel strips. J Build Eng 2023;69:106076.
[20] Borri A, Corradi M, Castori G, Molinari A. Stainless steel strip–a proposed shear reinforcement for masonry wall panels. Constr Build Mater 2019;211:594–604.
[21] Luan H-Y, Fan Y-F, Chen A, Zhang S-Y. Exploratory experimental study on flexural behavior of CFRP-reinforced concrete beams subjected to acidic loading effect. Adv Struct Eng 2018;21:2184–97.
[22] Tang H, Deng X, Lin Z, Zhou X. Analytical and experimental investigation on bond behavior of CFRP-to-stainless steel interface. Compos Struct 2019;212:94–105.
[23] SEI/ASCE-8-02. Specification for the design of cold-formed stainless steel structural members. Virginia, USA: American Society of Civil Engineers; 2002.
[24] EN1993-1-4. Design of steel structures-part 1-4: general rules-supplementary rules for stainless steels. Brussels, Belgium: European Committee for Standardization; 2006.
[25] AS/NZS 4673–2001. Cold-formed stainless steel structures.Sydney, NSW, Australia: Australian/New Zealand Standard; 2001.
[26] Franco N, Biscaia H, Chastre C. Experimental and numerical analyses of flexurally-strengthened concrete T-beams with stainless steel. Eng Struct 2018;172:981–96.
[27] Hamoda AA, Eltaly B, Ghalla MS. Numerical investigation on reinforced concrete closed curved beams subjected to internal pressure strengthened with sustainable material. Eng Res J 2023;46:233–47.
[28] Hamoda AA, Eltaly BA, Ghalla M, Liang QQ. Behavior of reinforced concrete ring beams strengthened with sustainable materials. Eng Struct 2023;290:116374.
[29] Ahmed S, Sharaky I, Ibrahim YE, Abdo A. Flexural response of GFRP RC beams strengthened with side and bottom NSM GFRP bars. Case Stud Constr Mater 2023;18:e01858.
[30] Hashemi SM, Riahi HT. Seismic performance of reinforced concrete beam-column joints strengthened with NSM steel bars and NSM CFRP strips. Structures 2022:57–69.
[31] Sharaky I, Elamary A, Alharthi Y. Experimental and numerical investigation on the flexural performance of RC slabs strengthened with EB/NSM CFRP reinforcement and bonded reinforced HSC layers. Eng Struct 2023;289:116338.
[32] Abdo A, Ahmed S, Selim M, Sharaky I. Effect of main and NSM reinforcing materials on the behavior of the shear strengthened RC beams with NSM reinforced HSC layers and bars. Case Stud Constr Mater 2023;18:e02109.

[33] Huang J, Xing G, Chang Z. Experimental and numerical investigation on flexural behavior of concrete beams strengthened by different NSM tendons. Compos Struct 2023;313:116947.
[34] Mansouri S, Morshed R, Mostofinejad D. Using NSM pre-stressed rebars for flexural strengthening of RC beams subjected to constant loading. Structures 2022;43:1478–91.
[35] Misnon NA, Giaretton M, Shedde D, Ingham J, Dizhur D. Shear testing of URM wallettes retrofitted with NSM steel wire rope. Structures 2020;27:1613–22.
[36] Bilotta A, Ceroni F, Di Ludovico M, Nigro E, Pecce M, Manfredi G. Bond efficiency of EBR and NSM FRP systems for strengthening concrete members. J Compos Constr 2011;15:757–72.
[37] Ma G, Wu C, Liu K. Seismic performance of lap-spliced pre-damaged and intact concrete columns strengthened or retrofitted with UHPC and NSM. Eng Struct 2023;277:115431.
[38] Al-Issawi ASH, Kamonna HH. Experimental study of RC deep beams strengthened by NSM steel bars. Mater Today Proc 2020;20:540–7.
[39] Lee HY, Jung WT, Chung W. Flexural strengthening of reinforced concrete beams with pre-stressed near surface mounted CFRP systems. Compos Struct 2017;163:1–12.
[40] Elsamak G, Salama MI, Hamoda A. Behavior of precast segmental beams made of high-strength concrete and ultra-high performance fiber concrete connected by shear keys technique. Arab J Sci Eng 2023;48:4907–23.
[41] Zhu P, Fan H, Zhou Y. Flexural behavior of aluminum I-beams strengthened by pre-stressed CFRP tendons. Constr Build Mater 2016;122:607–18.
[42] Rashid K, Li X, Deng J, Xie Y, Wang Y, Chen S. Experimental and analytical study on the flexural performance of CFRP-strengthened RC beams at various pre-stressing levels. Compos Struct 2019;227:111323.
[43] Miao W, Guo Z-X, Ye Y, Basha SH, Liu X-J. Flexural behavior of stone slabs strengthened with prestressed NSM steel wire ropes. Eng Struct 2020;222:111046.
[44] Sayed M, Elrakib T. Rehabilitation of reinforced concrete beams with insufficient longitudinal reinforcement lap-splice length using FRP sheets. Concrete Solutions 2011. CRC Press; 2011. p. 653–62.
[45] Beiter K.S. Retrofit of deficient lap splice with post-installed anchors; 2015.
[46] ACI 318–19-Building code requirements for reinforced concrete. American Concrete Institute; 2019.
[47] Dagenais M-A, Massicotte B. Tension lap splices strengthened with ultrahigh-performance fiber-reinforced concrete. J Mater Civ Eng 2015;27:04014206.
[48] Abdallah AM, Badawi M, Elsamak G, Hu JW, Mlybari EA, Ghalla M. Strengthening of RC beams with inadequate lap splice length using cast-in-situ and anchored precast ECC ferrocement layers mitigating construction failure risk. Case Stud Constr Mater 2024;20:e02747.
[49] Ge W, Ashour AF, Cao D, Lu W, Gao P, Yu J, et al. Experimental study on flexural behavior of ECC-concrete composite beams reinforced with FRP bars. Compos Struct 2019;208:454–65.
[50] Hamoda AA, Ahmed M, Abadel AA, Ghalla M, Patel VI, Liang QQ. Experimental and numerical studies of circular precast concrete slender columns with intermediate connection filled with high-performance concrete. Structures 2023;57:105204.
[51] Ghalla M, Mansour W, Li W, Wang P, Badawi M, El Zareef MA. Enhancing the punching performance of two-way RC flat slabs using different configurations of embedded aluminum sections: experimental program and numerical analysis. Constr Build Mater 2024;434:136737.
[52] Hibbitt K., Sorensen I. ABAQUS theory manual, user manual and example manual. Providence, RI, USA: Simulia; 2000.
[53] Fayed S, Basha A, Elsamak G. Behavior of RC stepped beams with different configurations: an experimental and numerical study. Struct Concr 2020;21:2601–27.
[54] Elsamak G, Fayed S. Parametric studies on punching shear behavior of RC flat slabs without shear reinforcement. Comput Concr 2020;25:355–67.
[55] Elsamak G, Abdullah A, Salama MI, Hu JW, El-Mandouh MA. Punching shear behavior of slabs made from different types of concrete internally reinforced with SHCC-filled steel tubes. Materials 2022;16:72.
[56] Basha A, Fayed S, Elsamak G. Flexural behavior of cracked RC beams retrofitted with strain hardening cementitious composites. KSCE J Civ Eng 2019;23:2644–56.
[57] El Zareef MA, Ghalla M, Hu JW, El-Demerdash WE. Damage detection of lightweight concrete dual systems reinforced with GFRP bars considering various building heights and earthquake intensities. Case Stud Constr Mater 2024;20:e03191.
[58] Alharthai M, Bahrami A, Badawi M, Ghalla M, Elsamak G, Abdelmgeed FA. Numerical study on enhancing shear performance of RC beams with external aluminum alloy plates bonded using steel anchors. Results Eng 2024;22:102143.
[59] Ghalla M, Badawi M, Mlybari EA, Hu JW. Enhancing shear strength of RC beams through externally bonded reinforcement with stainless-steel strips and FRCM jacket to mitigate the failure risk. Results Eng 2024:102246.
[60] Salama MI, Elayat A, Reda M, Elsamak G. Influence of concrete type on rigid pavement behavior under static loads. Innov Infrastruct Solut 2024;9:15.
[61] Hamoda A, Ahmed M, Ghalla M, Liang QQ, Abadel AA. Flexural performance of precast circular reinforced concrete members with intermediate connection filled with ultra-high-performance-concrete. Case Stud Constr Mater 2023:e02386.
[62] Hamoda A, Elsamak G, Emara M, Ahmed M, Liang QQ. Experimental and numerical studies of reinforced concrete beam-to-steel column composite joints subjected to torsional moment. Eng Struct 2023;275:115219.
[63] Gan Y. Bond stress and slip modeling in nonlinear finite element analysis of reinforced concrete structures. Toronto, ON, Canada: University of Toronto; 2000.
[64] Guo Z, Cao S, Sun W, Lin X. Experimental study on bond stress-slip behaviour between FRP sheets and concrete. FRP in construction. In: Proceedings of the international symposium on bond behaviour of FRP in structures 2005:77–84.
[65] Lu X, Teng J, Ye L, Jiang J. Bond–slip models for FRP sheets/plates bonded to concrete. Eng Struct 2005;27:920–37.
[66] Obaidat YT, Heyden S, Dahlblom O. The effect of CFRP and CFRP/concrete interface models when modelling retrofitted RC beams with FEM. Compos Struct 2010;92:1391–8.
[67] Galal Elsamak AHE, Basem ORageh. Numerical modelling of the behavior of bare and masonry-infilled steel frames with different types of connections under static loads. Comput Concr 2024;33:17.
[68] Magdy I, Salama JWH, Ahmed Almaadawy, Ahmed Hamoda, Rageh Basem O, Galal Elsamak. Behavior of simple precast high-strength concrete beams connected in the maximum bending moment zone using steel extended endplate connections. Steel Compos Struct 2024;50:15.
[69] EN1992–1-1, Design of concrete structures. Part 1–1: general rules and rules for buildings. russels, Belgium: European Committee for Standardization (CEN); 2004.